

Structure-Based Design, Synthesis, and Characterization of Dual Hotspot Small-Molecule HIV-1 Entry Inhibitors

Judith M. LaLonde,^{*,†,∞} Young Do Kwon,^{‡,∞} David M. Jones,^{§,∞} Alexander W. Sun,[§] Joel R. Courter,[§] Takahiro Soeta,[§] Toyoharu Kobayashi,[§] Amy M. Princiotto,^{||} Xueling Wu,[‡] Arne Schön,[⊥] Ernesto Freire,[⊥] Peter D. Kwong,[‡] John R. Mascola,[‡] Joseph Sodroski,^{||, #} Navid Madani,^{||} and Amos B. Smith, III^{*,§}

[†]Department of Chemistry, Bryn Mawr College, Bryn Mawr, Pennsylvania 19010, United States

[‡]Vaccine Research Center, National Institutes of Health, National Institute of Allergy and Infectious Diseases, Bethesda, Maryland 20892, United States

[§]Department of Chemistry, University of Pennsylvania, Philadelphia, Pennsylvania 19104, United States

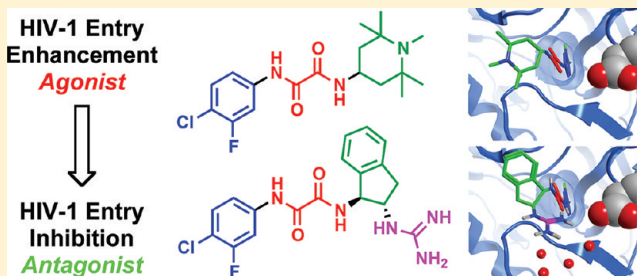
^{||}Department of Cancer Immunology and AIDS, Dana-Farber Cancer Institute, Harvard Medical School, 450 Brookline Avenue, Boston, Massachusetts 02115, United States

[⊥]Department of Biology, The Johns Hopkins University, Baltimore, Maryland 21218, United States

[#]Department of Microbiology and Immunology, Harvard Medical School; Department of Immunology and Infectious Diseases, Harvard School of Public Health; Ragon Institute of MGH, MIT and Harvard, Boston, Massachusetts 02115, United States

S Supporting Information

ABSTRACT: Cellular infection by HIV-1 is initiated with a binding event between the viral envelope glycoprotein gp120 and the cellular receptor protein CD4. The CD4–gp120 interface is dominated by two hotspots: a hydrophobic gp120 cavity capped by Phe43_{CD4} and an electrostatic interaction between residues Arg59_{CD4} and Asp368_{gp120}. The CD4 mimetic small-molecule NBD-556 (**1**) binds within the gp120 cavity; however, **1** and related congeners demonstrate limited viral neutralization breadth. Herein, we report the design, synthesis, characterization, and X-ray structures of gp120 in complex with small molecules that simultaneously engage both binding hotspots. The compounds specifically inhibit viral infection of 42 tier 2 clades B and C viruses and are shown to be antagonists of entry into CD4-negative cells. Dual hotspot design thus provides both a means to enhance neutralization potency of HIV-1 entry inhibitors and a novel structural paradigm for inhibiting the CD4–gp120 protein–protein interaction.



■ INTRODUCTION

Infection by the HIV-1 virus and the subsequent progression to AIDS^{1,2} begin with protein–protein binding events between the trimeric envelope glycoprotein spike (Env) and host cell receptors.^{3–7} Each trimeric Env spike is composed of three gp120 envelope glycoproteins and three gp41 transmembrane proteins.^{8–10} The HIV-1 viral entry process begins with two consecutive gp120–protein binding events, each associated with changes in Env conformation.^{7,11–13} Attachment of HIV occurs when gp120 binds to the T-cell CD4 receptor^{3,14} anchored to the cell membrane. Binding to CD4 then induces a gp120 conformational change,^{11,12} which exposes the binding site for the transmembrane chemokine co-receptor (CCR5 or CXCR4).^{15–17} Once co-receptor binding occurs, gp41 rearranges to form the six-helix bundle which inserts into the host cell membrane, culminating in fusion and viral entry.^{6,18–20}

Inhibition of the initial entry event of the HIV-1 virus into host cells remains a compelling, yet elusive means to prevent or treat HIV-1 infection and AIDS. Currently, only two

therapeutic agents that target the viral entry process are approved in the U.S. for the treatment of individuals infected with HIV-1: maraviroc,²¹ a small molecule CCR5-antagonist, and enfuvirtide,²² a 36-amino acid peptide that binds gp41 and prevents formation of the fusion peptide. Indeed, to date, limited progress has been made on developing inhibitors that target the initial step in viral entry, CD4–gp120 binding.^{23–26} Hence, disruption of the earliest CD4–gp120 protein–protein interactions at the host cell–viral interface remains an important, yet difficult strategy for blocking HIV-1 infection.

A number of X-ray crystal structures of the gp120 core bound to the D1D2 domains of CD4 and the Fab of the neutralizing antibody 17b, a surrogate for the co-receptor, have been solved.^{27–34} The structure of the unbound form of the simian immunodeficiency virus (SIV) gp120, which has a 35% sequence identity with HIV-1 gp120, indicates an invariant

Received: February 24, 2012

Published: April 12, 2012



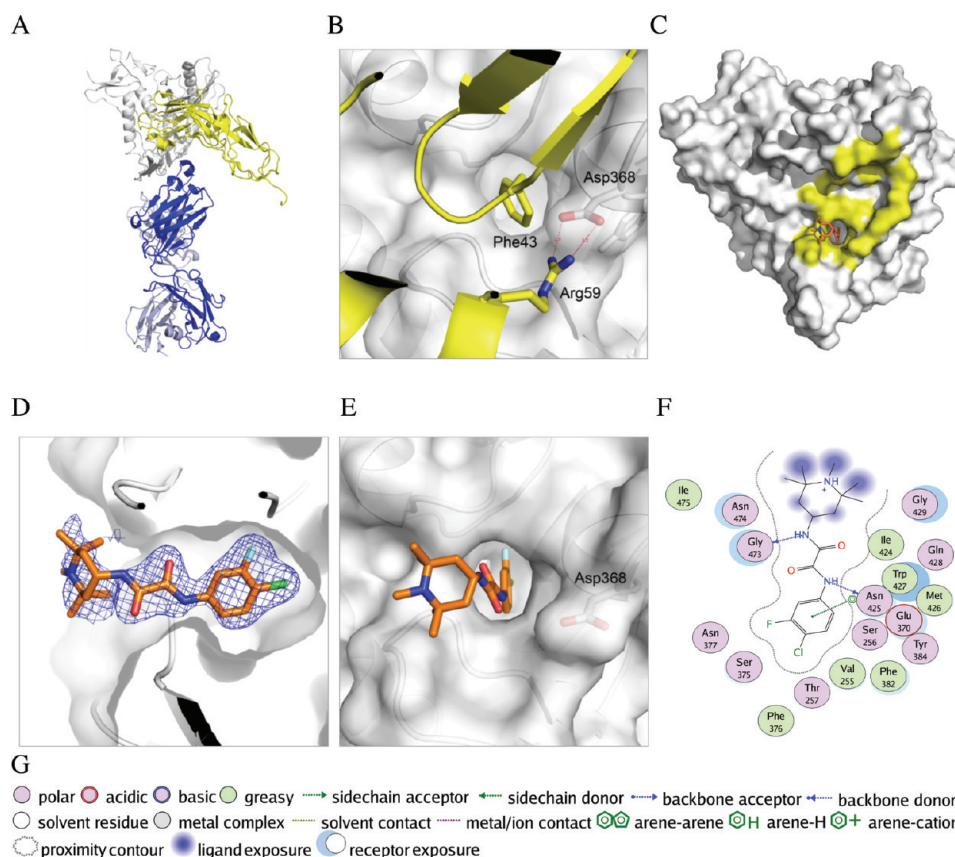


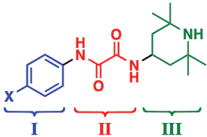
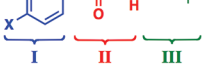
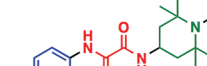
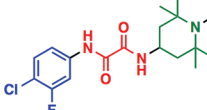
Figure 1. gp120–CD4 binding interface and crystal structure of gp120–4 complex: (A) X-ray crystal structure of the ternary gp120 (gray)–CD4 (yellow)–17Fab (blue/light blue) complex; (B) dual hotspot interactions observed in the native CD4–gp120 interaction, with Phe43_{CD4} (yellow) bound at the entrance to the Phe43 cavity with the adjacent salt bridge between Asp368_{gp120} and Arg59_{CD4}; (C) crystal structure of 4 (orange) bound in the Phe43 cavity of gp120_(H375S) core, with the CD4 binding footprint highlighted in yellow; (D) 2F_o – F_c electron density map of 4 contoured at 1σ; (E) position of 4 region III relative to Asp368_{gp120}; (F) 4–gp120 interaction map calculated and rendered with MOE ligand interaction utility;⁷³ (G) symbolic key for the ligand interaction map.

outer domain, with conformational differences in both the bridging sheet and inner domain.³⁵ In the ternary HIV-1 CD4–gp120–17b complex a large internal cavity is formed at the interface of the inner, outer, and bridging sheet domains of gp120 (Figure 1A).^{31,32} Furthermore, a recent crystallographic study of the unliganded HIV-1 gp120 monomeric core demonstrates the propensity of gp120 to assume the CD4-bound conformation when not restrained by the presence of variable loops and interactions with gp41 in the trimer spike.³⁶ At the CD4–gp120 interface, residue Phe43_{CD4} is located on the CDR2-like loop and binds within the hydrophobic cavity of gp120, termed the “Phe43 cavity”, while Arg59_{CD4} is located on a neighboring β -strand and forms an electrostatic interaction with Asp368_{gp120} (Figure 1B).^{31,32} Importantly, the amino acids lining the Phe43 cavity, as well as Asp368_{gp120}, are well-conserved among primary HIV-1 isolates.³⁷ Upon mutation of Phe43_{CD4} to Ala43_{CD4} a 550-fold reduction of binding affinity for gp120 was observed.³⁸ Equally significant, the protein–protein interaction is reduced 9-fold when Arg59_{CD4} is mutated to Ala. Thus, the mutagenesis data and high degree of residue conservation highlight the functionally critical role that both the Phe43 cavity and Asp368_{gp120} binding hotspots play in mediating the HIV-1 viral entry process. Although inhibition of protein–protein interactions continues to be a significant challenge,^{39–41} recent examples indicate that efficient inhibition can be achieved by targeting surface hotspots.^{39,42} The large CD4–gp120 contact surface, the orthogonal arrangement

between the Phe43 cavity and the Asp368_{gp120} hotspots, and the therapeutic potential of targeting this interface comprise a challenging opportunity to combine structure based design and synthesis to develop novel small molecule antagonists of the viral attachment and entry process.

Previous screening of a small-molecule library for inhibitors of viral fusion led Debnath and co-workers to identify two inhibitors of CD4–gp120 binding, NBD-556 (1) and NBD-557 (2) (Table 1).⁴³ Subsequent studies in our laboratories revealed that while 1 and 2 inhibit HIV-1 viral entry in CD4-positive, CCR5-expressing T-cells, 1 and 2 actually activate viral infection in CD4-negative cells (Table 1, column 3).⁴⁴ Thus, in the context of CD4-negative cells, these small molecules both function as surrogates of the CD4 receptor and serve as agonists by promoting HIV-1 entry. Promotion of HIV-1 entry by NBD compounds may be possible in CD4-independent HIV-1 variants,^{45,46} therefore, the agonistic properties of 1 and 2 must be eliminated for this chemotype. The thermodynamic signature of 1 binding to gp120 provides further evidence of the CD4-mimetic properties. For example, soluble CD4 (sCD4) binding to gp120 exhibits a highly favorable binding enthalpy balanced with an unfavorable entropy associated with molecular ordering.^{47,48} Binding of 1 to the gp120 core is also characterized by both a favorable change in enthalpy (ΔH) and a large, unfavorable entropic component ($-T\Delta S$) (Table 1).^{44,49} The similarity in thermodynamic signature for sCD4

Table 1. Tetramethylpiperidine Analogues

| Compound | HIV-1, YU-2 IC ₅₀ (μM) ^a | A-MLV IC ₅₀ (μM) ^b | Activation of Viral Infectivity ^c | K _d (μM) ^d | ΔG (kcal/mol) ^e | ΔH (kcal/mol) ^d | −TΔS (kcal/mol) ^f |
|---|---|---|---|-------------------------------------|-------------------------------|-------------------------------|---------------------------------|
|  NBD-556 (1) (X = Cl) ^g | >100 | >100 | 1.0 | 3.7 | −7.4 | −24.5 | +17.1 |
|  NBD-557 (2) (X = Br) ^g | >100 | >100 | 0.8 (relative to 1) | 2.2 | −7.7 | −22.8 | +15.1 |
|  JRC-I-191 (3) (R = H) ^h | 54.4 | >100 | 1.9 (relative to 1) | 0.76 | −8.3 | −20.8 | +12.5 |
|  TS-II-224 (4) (R = Me) | 48.8 ± 3.6 | 93.4 ± 1.9 | 2.1 (relative to 3) | 0.30 | −8.8 | −19.7 | +10.9 |

^aCompounds 1, 2, 3, and 4 were assayed in triplicate, and the data are reported as the mean with standard deviation for 1, 1, 1, and 52 experiments, respectively. The compound concentrations that inhibited 50% of virus infection (IC₅₀) were determined by infecting Cf2Th-CD4/CCR5 cells with 10 000 RT units of wild-type HIV-1_{YU2} virus expressing luciferase with increasing concentrations of the compound. ^bThe compound concentrations that inhibited 50% of virus infection (IC₅₀) when assayed against viruses with the amphotropic murine leukemia virus (A-MLV) envelope glycoproteins. ^cActivation of viral infectivity was determined by infecting Cf2Th-CCR5 cells with recombinant HIV-1_{YU2} in the presence of NBD analogues. The luciferase activity in the target cells incubated with each compound was divided by that in the cells incubated with 2 to obtain the relative activation of infectivity. ^dThe dissociation constant (K_d) and the change in enthalpy (ΔH) were determined at 25 °C by isothermal titration calorimetry using a high-precision VP-ITC titration calorimetric system from MicroCal/GE Healthcare (Northampton, MA, U.S.). The calorimetric cell (approximately 1.4 mL), containing gp120 from the YU2 strain dissolved in PBS (Roche Diagnostics GmbH, Mannheim, Germany), pH 7.4, with 2% DMSO, was titrated with the different inhibitors dissolved in the same buffer. The concentration of gp120 was approximately 2 μM, and inhibitor at a concentration of 80–130 μM was added in aliquots of 10 μL until saturation was reached (usually in 20–30 injections). ^eThe change in Gibbs energy (ΔG) was calculated from the affinity according to the relation ΔG = −RT ln K_a, where K_a is the association constant (K_a = 1/K_d), R is the gas constant (1.987 cal/(K·mol)), and T is the absolute temperature in kelvin. ^fTΔS was calculated from the relation ΔG = ΔH − TΔS. ^gData for 1–3 as reported in Schön et al.⁴⁹ and Madani et al.⁴⁴

and 1 suggests that the small molecules both induce and stabilize gp120 in a CD4-bound-like conformation.

SAR studies identified three pharmacophoric elements that define the NBD chemotype: region I, a para-halogenated phenyl ring; region II, the oxalamide linker; region III, a tetramethylpiperidine ring.^{44,50–52} Initial optimization of regions I and II^{44,51} led to the synthesis of JRC-I-191 (3) with improved binding affinity.⁵³ Mutagenesis and modeling of 3 revealed that these small molecules bind to the highly conserved gp120 cavity and compete with CD4 binding.^{44,49,51,54} Unexpectedly, we found that 3 inactivates HIV-1 by inducing irreversible conformational changes that result in an active, yet transient, intermediate state of the Env trimer. If the metastable trimer does not encounter a target cell within the lifetime of the activated intermediate, it decays to a state that is no longer competent for viral entry.⁵⁵ Further optimization of 3 led to the synthesis and biological evaluation of TS-II-224 (4), the most potent inhibitor of CD4–gp120 binding possessing the NBD chemotype.^{44,51} While analogues 3 and 4 have improved affinities for gp120, as measured by isothermal titration calorimetry (ITC), they are also more effective agonists of viral entry (relative to 1) in CD4-negative cells, clearly an undesired property (Table 1).^{44,51} The recent cocrystal structure of 1 bound to gp120 (clade C1086), at a resolution of 3.0 Å, confirms that 1 binds within the conserved Phe43 cavity.³⁶ However, 1 does not form specific interactions with Asp368_{gp120} at the second binding hotspot. Thus, the essential Arg59_{CD4}–Asp368_{gp120} electrostatic interaction on the CD4–gp120 surface has yet to be integrated in NBD small-molecule design. Hence, we hypothesized that engaging the Asp368_{gp120} binding hotspot would significantly improve viral inhibition properties while also targeting a residue that is well-conserved across many HIV-1 subtypes.³⁷ Herein, we describe a computational approach for the design of region III analogues that target both the Phe43 cavity and the Asp368_{gp120} hotspots.

RESULTS AND DISCUSSION

X-ray Crystallographic Characterization of 4 Bound to the Core of gp120. Recently, Kwon et al. determined four structures of the unliganded gp120 “extended core” (core_e) from clade B (YU2 strain), clade C (C1086 and ZM109 strains), and clade A/E (93TH057 strain) primary HIV-1 isolates.³⁶ The gp120 core_e includes the N-terminus but excludes the variable loops and facilitates crystallization of the unliganded gp120. The clade A/E_{93TH057} construct of gp120 core_e produced the highest resolution structure (1.9 Å).³⁶ This protein also produced well diffracting crystals in complex with VRC01-like antibodies.^{34,56} Therefore, we employed the same clade A/E gp120 core_e as a template for small molecule cocrystallizations, with the exception that we mutated His375 to Ser within the Phe43 cavity to accommodate ligand binding. The crystal structure of 4 bound to clade A/E gp120_(H375S) core_e was determined at 2.0 Å resolution by molecular replacement (Figure 1C–E and Table 3). This structure reveals that 4 binds similarly to 1 in the ligand–gp120 complex,³⁶ with region I bound deep within the Phe43 cavity and forming aromatic stacking interactions with Phe382_{gp120} and Trp427_{gp120}, as well as hydrophobic contacts with Val255_{gp120} and Ile424_{gp120}. Both amide nitrogens of region II form hydrogen bonds with the main-chain carbonyls on opposite sides of the Phe43 cavity (Gly473_{gp120} from the outer domain and with Asn425_{gp120} from the bridging sheet domain). In the cavity vestibule, one region III gem-dimethyl moiety forms van der Waals contacts with the bridging sheet domain residues Trp427_{gp120}, Asn428_{gp120}, and Glu429_{gp120}, while the second geminal dimethyl group contacts the outer domain residues Gln473_{gp120} and Asn474_{gp120}. This cocrystal structure was employed as the starting point for our virtual screening and inhibitor design efforts.

Structure Based Design. On the basis of the critical role of the Arg59_{CD4}–Asp368_{gp120} electrostatic interaction in CD4–gp120 recognition and binding,³⁸ we hypothesized that addition of a similar chemotype to region III, directed toward the Asp368_{gp120} hotspot, would improve the viral inhibition properties of **4**. The cocrystal structure of **4** bound to the clade A/E gp120_(H375S) core_c indicated the proximity of C4 of the tetramethylpiperidine ring (region III) and the carboxylate side chain of Asp368_{gp120} (Figure 1E). Rather than performing systematic synthetic modifications of region III congeners, we chose a virtual screening strategy to identify alternative scaffolds that would contain a basic amine oriented toward Asp368_{gp120}. Hence, an analogue possessing a primary amine attached to C4 of the 4-aminotetramethylpiperidine was constructed in silico to afford query structure **5** (Figure 2). While geminal diamine **5**

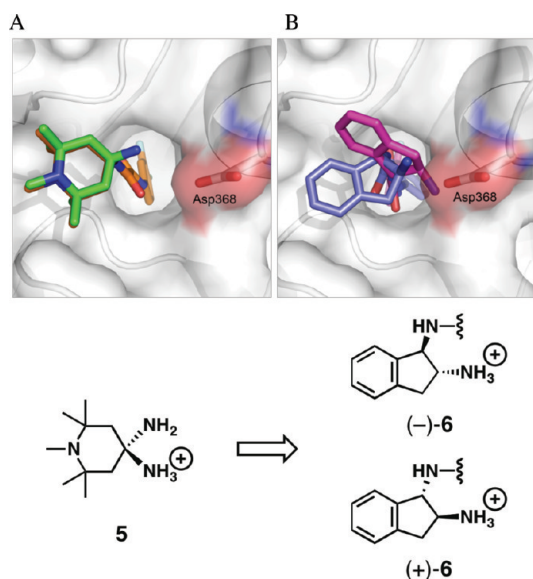


Figure 2. Structure-based design strategy: (A) crystal structure of **4** (orange) bound to gp120 and the docked model of the germinal diamine prototype **5** (green) used as a query in ROCS shape-based virtual screening; (B) docked conformations of the *trans*-1,2-diaminoindane isomers [**(-)-6** and **(+)-6**] (magenta and light blue, respectively) appended to the regions I and II scaffold of **4**.

is not a chemically stable entity, we exploited this archetype to replicate the desired interactions between the small molecule and gp120. The prototype was assessed with the docking program GOLD^{57,58} to provide a three-dimensional model that incorporated the desired trajectory of the amino group. Following our previously reported virtual screening paradigm⁵¹ employing the ROCS shape-based similarity algorithm,^{59–61} the amine prototype was used to search the ZINC database of commercially available compounds.^{62,63} Virtual screening identified several bicyclic primary amines, such as amino-bicyclononanol, indanol, and diaminoindanes, that displayed both shape and chemotype similarity to prototype **5** and directed a hydrogen bond donor toward Asp368_{gp120} (Table S1 in Supporting Information). In the end, we chose the synthetically versatile indane scaffold and docked the 1,2- and 1,3-diaminoindane enantiomers with GOLD.^{57,58} The *trans*-1,2-diaminoindane isomers **(-)-6** and **(+)-6** were predicted to form weak polar interactions with Asp368_{gp120} and thus were selected for synthesis (Figure 2).

Chemistry. To assess the suitability of the 1,2-diamines as region III platforms, we began with the synthetic conjugation of the commercially available *cis*-1-aminoindan-2-ol **(-)-8** to ethoxalamide **7** (Figure 3). Amide bond formation was achieved under thermal conditions to furnish **(+)-9**. Enantiomer **(-)-9** was also prepared employing the same procedure, beginning with **(+)-8**. These *cis*-indanol enantiomers **(+)-9** and **(-)-9** exhibited weak inhibition of viral entry (data not shown). Given that the *trans*-1,2-diaminoindanes exhibited the requisite spatial arrangement in the docking studies, we next converted **(+)-9** to the corresponding *trans*-amine **(+)-6**. Tosylation of alcohol **(+)-9** followed by S_N2 displacement with sodium azide furnished **(+)-10**. Reduction of the azide employing Lindlar's catalyst then provided the desired amine AWS-I-45 [**(-)-6**]. An identical synthetic sequence, beginning with **(+)-9**, was employed to construct the enantiomer AWS-I-50 [**(+)-6**]. Although **(-)-6** and **(+)-6** exhibited nonspecificity in our standard viral-entry inhibition assays (vide infra), conversion of the alcohol to the amines demonstrated an increase in binding affinity [K_d (**(-)-6**) = 1.2 μ M; K_d (**(+)-6**) = 1.9 μ M] compared to **1** (K_d = 3.7 μ M). Encouraged by this result, we sought to mimic further the Arg59_{CD4} side chain. Assessment of guanidine analogues by docking predicted favorable interactions between

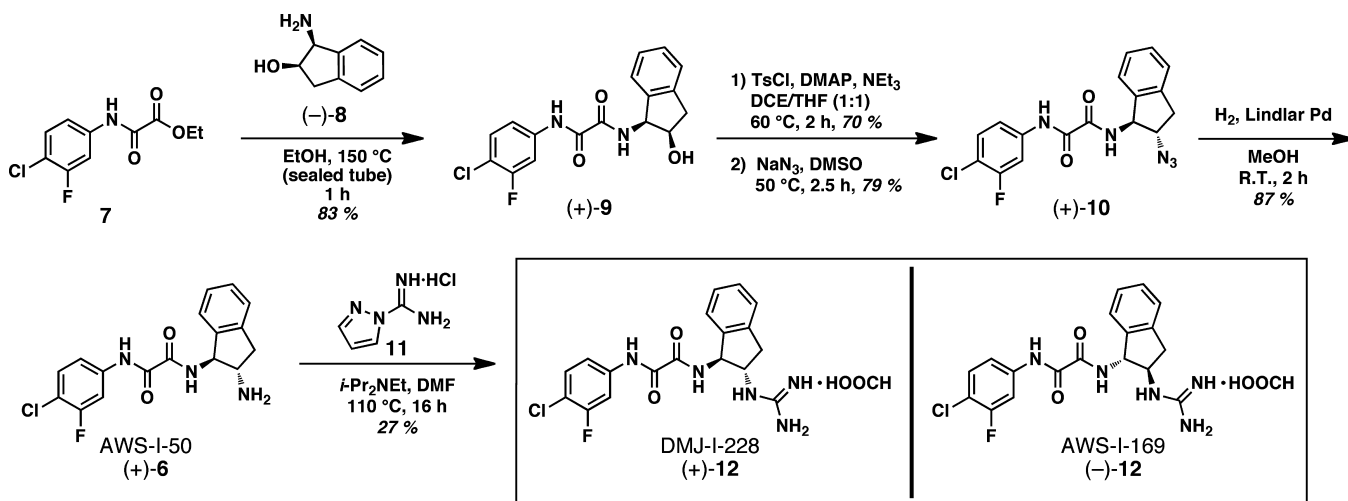
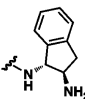
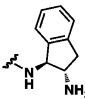
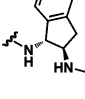
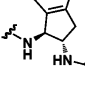


Figure 3. Synthesis of the guanidinium analogues **(-)-12** and **(+)-12**.

Table 2. Indane Analogues

| Compound | HIV-1, YU-2 IC ₅₀ (μM) ^a | A-MLV IC ₅₀ (μM) ^b | Activation of Viral Infectivity ^c | K _d (μM) ^d | ΔG (kcal/mol) ^e | ΔH (kcal/mol) ^d | −TΔS (kcal/mol) ^f |
|--|---|---|---|-------------------------------------|-------------------------------|-------------------------------|---------------------------------|
|  (−)-6 | 86.9 ± 8.0 | 85.9 ± 8.8 | 1.0 ± 0.3 (relative to 4) | 1.1 | −8.1 | −19.5 | +11.4 |
|  (+)-6 | 53.9 ± 10.2 | 56.9 ± 11.4 | 1.4 ± 0.5 (relative to 4) | 1.9 | −7.9 | −15.4 | +7.6 |
|  (−)-12 | 21.3 ± 5.0 | > 100 | 0.0 ± 0.0 (4) (relative to 4) | 0.30 | −9.0 | −19.4 | +10.4 |
|  (+)-12 | 22.9 ± 2.4 | > 100 | 0.1 ± 0.0 (19) (relative to 4) | 0.25 | −9.0 | −14.9 | +5.6 |

^aCompounds (−)-6, (+)-6, (−)-12, and (+)-12 were assayed in triplicate, and the data are reported as the mean with standard deviation for 5, 6, 7, and 32 experiments, respectively. ^bThe compound concentrations that inhibited 50% of virus infection (IC₅₀) when assayed against viruses with the amphotrophic murine leukemia virus (A-MLV) envelope glycoproteins. ^cActivation of viral infectivity was determined by infecting Cf2Th-CCR5 cells with recombinant HIV-1_{YU2} in the presence of NBD analogues. The luciferase activity in the target cells incubated with each compound was divided by that in the cells incubated with 2 to obtain the relative activation of infectivity. ^dThe dissociation constant (K_d) and the change in enthalpy (ΔH) were determined at 25 °C by isothermal titration calorimetry using a high-precision VP-ITC titration calorimetric system from MicroCal/GE Healthcare (Northampton, MA, U.S.). The calorimetric cell (approximately 1.4 mL), containing gp120 from the YU2 strain dissolved in PBS (Roche Diagnostics GmbH, Mannheim, Germany), pH 7.4, with 2% DMSO, was titrated with the different inhibitors dissolved in the same buffer. The concentration of gp120 was approximately 2 μM, and inhibitor at a concentration of 80–130 μM was added in aliquots of 10 μL until saturation was reached (usually in 20–30 injections). ^eThe change in Gibbs energy (ΔG) was calculated from the affinity according to the relation ΔG = −RT ln K_a, where K_a is the association constant (K_a = 1/K_d), R is the gas constant (1.987 cal/(K·mol)), and T is the absolute temperature in kelvin. ^fTΔS was calculated from the relation ΔG = ΔH − TΔS.

the ligand and Asp368_{gp120}. These analogues were thus selected for synthesis. Here we employed 1H-pyrazol-1-carboxamide monohydrochloride (11) to convert amine (+)-6 and the corresponding enantiomer (−)-6 to the desired guanidinium functionality, affording AWS-I-169 [(−)-12] and DMJ-I-228 [(+)-12], respectively. Note that following purification by high performance liquid chromatography (HPLC), the guanidinium formate salts of (−)-12 and (+)-12 were isolated and employed in all biological assays. The synthesis of (+)-12 is illustrated in Figure 3.

Evaluation of Viral Inhibition. Amines (−)-6 and (+)-6 and the corresponding guanidinium salts (−)-12 and (+)-12 were first tested against monotropic and dual-tropic HIV-1 strains in single-round infection of recombinant HIV-1, encoding firefly luciferase.⁶⁴ The recombinant viruses employed were pseudotyped with HIV-1 envelope glycoproteins derived from either a CXCR4, laboratory-adapted HXBc2 isolate, or the CCR5, primary YU2 isolate. To evaluate compound specificity for HIV-1, the viruses were pseudotyped with the envelope glycoproteins of the amphotropic murine leukemia virus (A-MLV), an unrelated retrovirus.⁵³ In both monotropic (HXBc2, YU2, ADA, JRFL) and dual-tropic (89.6 and KB9) viruses, (−)-6 and (+)-6 inhibited entry on cells coexpressing CD4 and CCR5 or CXCR4 with IC₅₀ in the range 50–90 μM but also exhibited nonspecificity by inhibiting entry of the A-MLV control virus with a similar IC₅₀ (Table 2). The guanidinium salts (−)-12 and (+)-12, on the other hand, demonstrated improved inhibition of viral entry (22.9 and 21.3 μM, respectively). Moreover, the inhibition proved to be completely specific to HIV-1, as neither compound was found to inhibit

entry of A-MLV (Table 2 and Figure 4). Assessment of the *in vitro* cytotoxicity of (+)-12 in Cf2Th-CD4-CCR5 cells did not demonstrate measurable inhibition of cell growth (Figure S1 in Supporting Information). Thus, analogues (−)-12 and (+)-12 possess significantly improved antiviral activities relative to the starting compounds 1–4.

To characterize further the antiviral breadth, (−)-12 and (+)-12 were tested against 42 diverse HIV-1 strains (clades B and C). While the parent compound 1 was found to neutralize HIV-1 with a geometric mean titer (GMT) IC₅₀ = 29.3 μM, only 12% of isolates were found to have IC₅₀ < 10 μM (Figure 5 and Table S3 in Supporting Information). In contrast, both (−)-12 and (+)-12 were found to display 100% neutralization breadth among the viral isolates tested. Compound (−)-12 possessed a GMT IC₅₀ of 8.9 μM with 52% of the viral isolates having IC₅₀ < 10 μM. Similarly, (+)-12 revealed a mean IC₅₀ of 7.9 μM with 57% of the isolates having IC₅₀ < 10 μM. Compounds (−)-12, (+)-12, and 1 all exhibited less antiviral activity against clade C viruses compared to clade B strains. Given the high degree of sequence conservation in the Phe43 cavity and that the gp120 trimer exhibits a high degree of conformational diversity in solution,^{48,65,66} the decreased potency in clade C is not easily assignable.

Given the broadly neutralizing capabilities of the indane-based analogues, we asked if (−)-12 and (+)-12 could pose a therapeutic disadvantage by functionally replacing CD4 and enhancing cellular infection. We have previously measured the enhancement of HIV-1 entry in CD4-independent viruses, demonstrating that 1–4 enhance the entry of HIV-1 YU2 viruses in CD4-negative cells (*vide supra*).^{44,51} We found that

Table 3. Data Collection and Refinement Statistics

| | 4 | (+)-6 | (-)-12 | (+)-12 |
|-------------------------------------|---------------------------------|----------------------------------|----------------------------------|-----------------------------------|
| | Data Collection | | | |
| space group | $P2_1$ | $P2_1$ | $P2_1$ | $P2_12_12_1$ |
| cell dimension | | | | |
| <i>a</i> , <i>b</i> , <i>c</i> (Å) | 64.72, 68.90, 94.51 | 64.66, 68.48, 94.74 | 65.44, 68.60, 94.54 | 63.74, 67.52, 89.25 |
| α , β , γ (deg) | 90, 91.23, 90 | 90.0, 91.60, 90 | 90, 91.38, 90 | 90, 90, 90 |
| resolution (Å) | 50–2.0 (2.03–2.00) ^a | 50–1.80 (1.83–1.80) ^a | 50–1.80 (1.83–1.80) ^a | 46.3–1.88 (1.9–1.88) ^a |
| R_{sym} | 0.09 (0.49) ^a | 0.06 (0.59) ^a | 0.08 (0.57) ^a | 0.09 (0.37) ^a |
| $I/\sigma(I)$ | 11.5 (1.5) ^a | 19.4 (1.1) ^a | 17.5 (1.8) ^a | 34.7 (2.5) ^a |
| completeness (%) | 94.1 (74.0) ^a | 97.0 (72.9) ^a | 93.3 (55.0) ^a | 97.4 (72.1) ^a |
| redundancy | 3.1 (1.9) ^a | 3.3 (1.9) ^a | 6.5 (3.2) ^a | 5.2 (2.0) ^a |
| | Refinement | | | |
| resolution (Å) | 41–1.98 | 33.7–1.79 | 33.7–1.80 | 46.3–1.88 |
| no. reflections | 53979 | 74205 | 72604 | 29830 |
| $R_{\text{work}}/R_{\text{free}}$ | 20.3/23.8 | 19.8/22.4 | 18.8/20.8 | 19.3/23.3 |
| no. atoms | | | | |
| protein | 5308 | 5308 | 5308 | 2654 |
| ligand/ion | 388 | 384 | 392 | 196 |
| water | 394 | 479 | 443 | 198 |
| <i>B</i> factor | | | | |
| protein | 43.9 | 41.0 | 46.0 | 34.0 |
| ligand/ion | 67.2 | 59.3 | 61.1 | 47.0 |
| water | 42.8 | 42.5 | 45.4 | 39.8 |
| rmsd | | | | |
| bond length (Å) | 0.002 | 0.002 | 0.002 | 0.007 |
| bond angle (deg) | 0.663 | 0.699 | 0.644 | 0.869 |
| PDB entry | 4DKO | 4DKP | 4DKR | 4DKQ |

^aValues in parentheses are for the highest-resolution shell.

both amines (–)-6 and (+)-6 enhanced viral entry in CD4-negative cells at levels comparable to those previously measured for 1–4 (Table 2). Remarkably, the guanidinium salts (–)-12 and (+)-12 displayed no appreciable entry enhancement of YU2 viruses into CD4-negative, CCR5-expressing cells (Table 2). We further evaluated whether the lack of viral enhancement might be related to the unproductive binding of (–)-12–gp120 or (+)-12–gp120 complexes to the CCR5 receptor. Surface plasmon resonance (SPR) assessment of the CCR5 antibody surrogate 17b binding to the small molecule–gp120 complexes indicated that both 4 and the indane congeners [(–)-6, (+)-6, (–)-12, and (+)-12] enhance binding of 17b to both the monomeric core and full-length gp120 (Figure S2 in Supporting Information). Therefore, the enhancement of viral entry into CD4-negative, CCR5-expressing cells is likely unrelated to the formation of the 17b binding epitope. Hence, the addition of the guanidinium functionality reduces the undesired enhancement of viral infection observed for 1–4, (–)-6, and (+)-6. We therefore conclude that (–)-12 and (+)-12 function as viral entry antagonists in the context of CD4-negative cells expressing the CCR5 co-receptor.

Thermodynamic Signature of Small Molecule Antagonist Binding. The binding of the novel analogues to full-length gp120 from the YU2 strain was next characterized by ITC. The measured binding affinities of (–)-12 ($K_d = 0.30 \mu\text{M}$) and (+)-12 ($K_d = 0.25 \mu\text{M}$) demonstrate that incorporation of the guanidinium functionality restores potency comparable to that of parental compound 4 ($K_d = 0.30 \mu\text{M}$) (Table 2). We also note that the observed discrepancies between measured IC_{50} and K_d values (Table 2) reflect the differences in small molecule binding to the full Env trimer and the gp120 monomer in viral and ITC binding assays,

respectively. The binding efficiency index (BEI) is defined as the binding affinity (K_d) divided by molecular weight, while the surface efficiency index (SEI) is defined as the binding affinity (K_d) divided by the molecular polar surface area.⁶⁷ Both (–)-12 and (+)-12, with identical affinity and structural properties, yield the same calculated BEI and SEI, 16.8 and 6.4, respectively. When compared to 22 known inhibitors of protein–protein interactions (BEI = 11.7 ± 2.4 and SEI = 7.2 ± 3.0)^{41,68} and 92 marketed drugs, (BEI = 25.8 ± 7.9 and SEI = 14.5 ± 8.7), the values for (–)-12 and (+)-12 fall within the lower bounds of binding efficiency and surface efficiency space for marketed drugs.⁶⁷

We next assessed the enthalpic and entropic contributions to binding compared to sCD4 binding (Table 2 and Figure 6A). The binding of sCD4 to gp120 at 25 °C is associated with a large enthalpy change ($\Delta H = -34.5 \text{ kcal/mol}$) that is partially negated by a large unfavorable entropy change ($-T\Delta S = 23.6 \text{ kcal/mol}$) and is associated with a large negative heat capacity (ΔC_p) of $-1800 \text{ cal/(K}\cdot\text{mol)}$.⁴⁹ Such a binding event suggests a large molecular reordering of gp120 upon CD4 binding.^{48,49} Compounds 1–4 also exhibit a large unfavorable entropy upon binding to gp120.⁴⁹ Thus, these small molecules bind and stabilize a gp120 conformation similar to that observed in the CD4 bound state. Characterization of analogues (–)-6 and (–)-12 (Table 2) indicated a thermodynamic signature resembling that of 4 (Figure 6B and Table 2). Conversely, the antipodes (+)-6 and (+)-12 exhibited decreased unfavorable entropy contributions ($-T\Delta S = 7.6$ and 5.9 kcal/mol , respectively) compared to 1–4, (–)-6, and (–)-12. Therefore, the (+)-6 and (+)-12 enantiomers, as shown in Figure 6, have a distinct and preferable thermodynamic signature, with gp120 incurring a lower entropic penalty upon binding. The

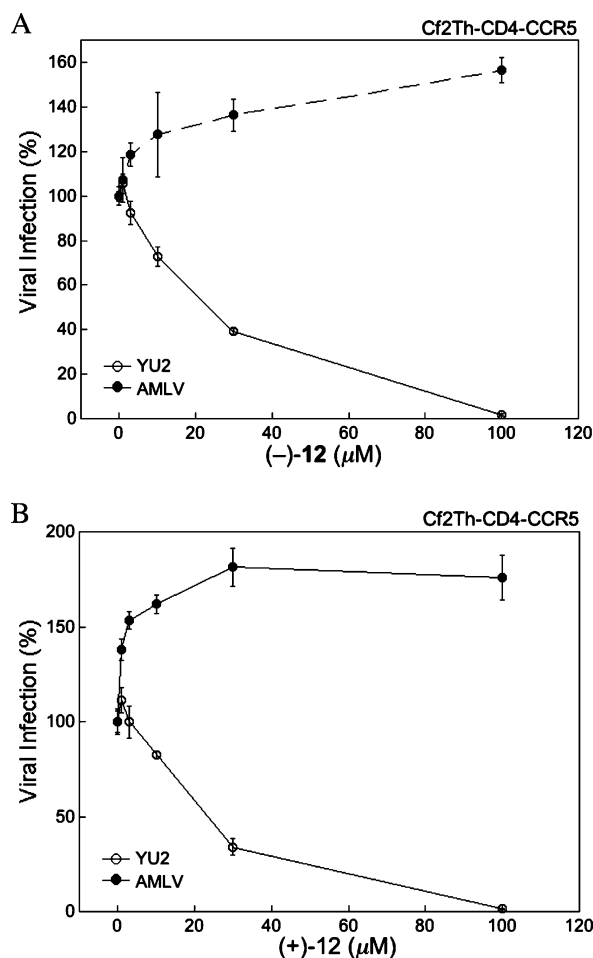


Figure 4. Virologic assessment of guanidinium analogues (–)-12 and (+)-12: (A) effect of (–)-12 on the infection of Cf2Th-CD4-CCR5 cells by recombinant luciferase-expressing HIV-1 envelope glycoproteins of the YU2 strain of HIV-1 or the amphotropic murine leukemia virus (AMLV); (B) effect of (+)-12 on the infection of Cf2Th-CD4-CCR5 cells by recombinant luciferase-expressing HIV-1 envelope glycoproteins of the YU2 strain of HIV-1 or AMLV. Virus infection is expressed as the percentage of infection (measured by luciferase activity in the target cells) observed in the presence of increasing concentrations of (–)-12 or (+)-12 relative to the level of infection observed in the absence of compound. The results are representative of 17 independent experiments. Additional data are provided in Tables S2 and S3 in Supporting Information.

associated changes in heat capacity for the binding of 4, (–)-12, and (+)-12, calculated from the temperature dependence of the binding enthalpies, are -738 ± 36 , -817 ± 15 , and -398 ± 5 cal/(K·mol), respectively (Figure 6B). The change in the heat capacity for (+)-12 approaches the expected value for the burial of a small hydrophobic molecule.^{69,70} Thus, enantiomer (+)-12 displays chemical properties and a thermodynamic signature resembling small molecule drug binding.

To determine if the antiviral and thermodynamic properties of (–)-12 and (+)-12 were exerted through direct binding to the Phe43 cavity hotspot, we measured viral inhibition in the Phe43 cavity filling mutant S375W_{gp120} YU2 virus, wherein the tryptophan side chain restricts access to the Phe43 cavity.⁷¹ Unlike the wild-type virus, the YU2 S375W_{gp120} was completely resistant to (–)-12 and (+)-12 (Table S2 in Supporting Information), supporting the claim that these new compounds exhibit their antiviral effects through binding within the

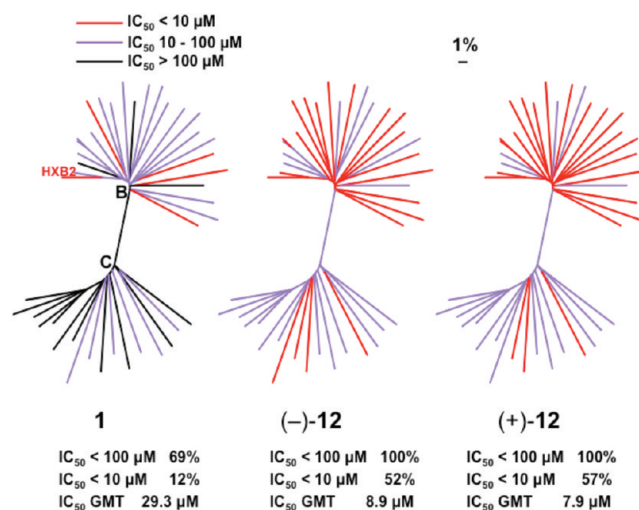


Figure 5. Comparison of neutralization by 1, (–)-12, and (+)-12 against HIV-1 Env-pseudoviruses. Dendrograms are made by the neighbor-joining method, showing the protein distance of gp160 sequences from 42 HIV-1 clades B and C isolates. The clade B reference strain HXB2 was used to root the tree, and the amino acid distance scale is indicated with a value of 1% distance as shown. Neutralization potency of 1, (–)-12, and (+)-12 is indicated by the color of the branch for each virus. The data under the dendrograms show the percent of viruses neutralized with IC₅₀ < 100 μM and IC₅₀ < 10 μM and the IC₅₀ geometric mean titer (GMT) for viruses neutralized with IC₅₀ < 100 μM. Data are included in Table S3 in Supporting Information.

conserved Phe43 cavity in the context of the functional trimeric Env spike. Cococrystallization experiments with compounds (+)-6, (–)-12, and (+)-12 bound to the monomeric A/E gp120_(H375S) core_e were employed to define further the binding interactions of these small molecule ligands with gp120.

Structural Characterization of Small Molecule–gp120 Interactions by X-ray Crystallography. Amine (+)-6 and guanidinium salts (–)-12 and (+)-12 were cococrystallized in complex with the clade A/E gp120_(H375S) core_e and yielded high resolution X-ray cocrystal structures at 1.8, 1.8, and 1.9 Å, respectively (Figures 7, 8, and 9 and Table 3).⁷² In the three crystal structures, regions I and II maintain similar interactions, as observed with 4, binding deep within the Phe43 cavity of gp120 (Figures 7, 8, and 9). The mean rmsd values of the backbone and side chain atoms for residues lining the Phe43 cavity are 0.39 and 0.68 Å, respectively, indicating structural conservation in the Phe43 hotspot among the ligand–gp120 complexes. Moreover, comparison of the (+)-6–gp120, (–)-12–gp120, or (+)-12–gp120 complex with the unliganded gp120 structure³⁶ or the CD4–gp120 structure (PDB code 1G9M)³¹ shows that the Asp368_{gp120} side chain has the same orientation upon small molecule binding. Inspection of region III in the (+)-6–gp120 complex (Figure 7) reveals that the 2-amino group does not interact with the Asp368_{gp120} hotspot. Nonetheless, the indane scaffold of (+)-6 occupies a similar position to the tetramethylpiperidine ring of 4 (Figure S3A in Supporting Information). The five-membered ring of (+)-6 overlaps with the piperidine ring, while the aromatic ring overlaps with one of the gem-dimethyl groups of 4 (Figure S3A in Supporting Information). The aromatic ring of (+)-6 also forms extensive contacts with outer domain residues Gly473_{gp120} and Asn474_{gp120}. Superposition of the (+)-6–

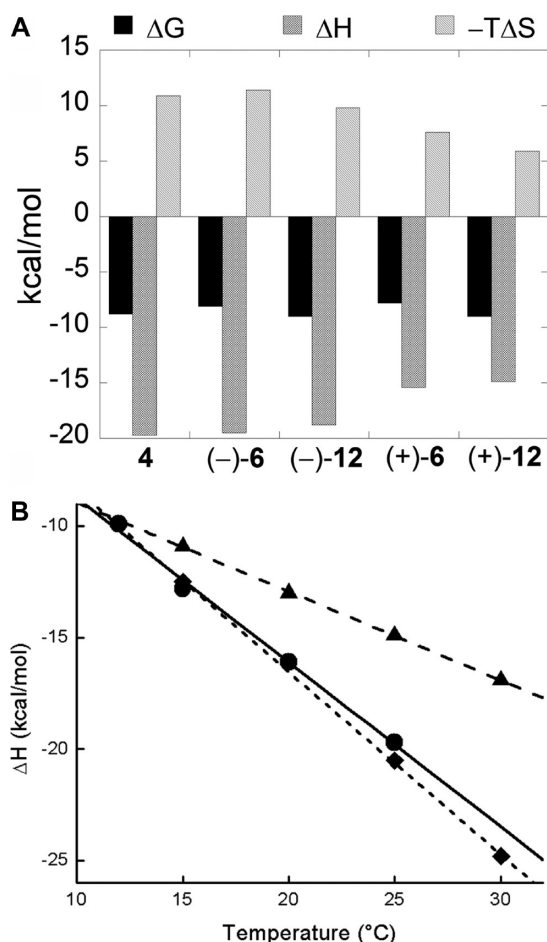


Figure 6. Thermodynamic characterization of indanes. (A) Gibbs energy (ΔG) and the enthalpic (ΔH) and entropic ($-T\Delta S$) contributions are compared for the binding of 4, (-)-6, (+)-6, (-)-12, and (+)-12 to full-length monomeric gp120 at 25 °C. (B) The temperature dependence of ΔH for 4 (circles), (-)-12 (squares), and (+)-12 (triangles) is shown. The changes in heat capacity, calculated from linear regression of the slopes, are -738 ± 36 cal/(K·mol) for 4 (solid line), -817 ± 15 cal/(K·mol) for (-)-12 (short dashed line), and -398 ± 5 cal/(K·mol) for (+)-12 (dashed line).

gp120 structure with a CD4–gp120 structure indicates that the indane arene ring overlaps with Asn40_{CD4} and Gly41_{CD4} main-

chain atoms, while the five-membered ring overlaps with the main-chain atoms of Ser42_{CD4} and Phe43_{CD4} (Figure S3A and S3B in Supporting Information). Therefore, the indane ring effectively mimics the CD4 β -turn spanning the interface of the outer domain and bridging sheet of gp120.

Addition of the guanidinium group to afford (-)-12 and (+)-12 was envisioned to strengthen the ligand interactions with the Asp368_{gp120} hotspot to resemble more closely the native protein–protein interaction. The 1.8 Å cocrystal structure of the (-)-12–gp120 complex reveals that the indane ring is rotated 90° in the cavity vestibule (relative to region II), leaving the plane of the ring tilted away from the gp120 surface (Figure 8). Hence, the arene ring of (-)-12 does not form contacts with the outer domain as observed in the (+)-6–gp120 complex (Figure 8). Furthermore, the altered orientation imposed by the stereochemical configuration of (-)-12 dictates that the guanidinium functionality approach Asp368_{gp120} near the outer domain rather than near the bridging sheet as observed with (+)-6. Interestingly, the guanidinium moiety of (-)-12 does not form a salt bridge with Asp368_{gp120}. Instead, the guanidinium group forms hydrogen bonds with a network of ordered water molecules (Wat601–Wat603) and forms a single ionic interaction with Asp368_{gp120} (Figure 8). Therefore, in the (-)-12–gp120 complex, the guanidinium moiety resides at the center of a hydrogen-bonded network between ordered watered and the outer domain residues Gly472_{gp120} and Asp368_{gp120}.

Further analysis of the (+)-12–gp120 cocrystal structure indicates that the guanidinium group of (+)-12 approaches Asp368_{gp120} between the bridging sheet and outer domains (Figure 9). The guanidinium moiety of (+)-12 also forms a single ionic interaction with Asp368_{gp120} and in addition forms an intramolecular hydrogen bond to the region II oxalamide and a hydrogen bond to crystallographic water Wat501. Interestingly, Wat501 occupies a position equivalent to that of Arg59_{CD4} observed in the CD4–gp120 complex (Figure S3B in Supporting Information).³¹ Wat501 is at the center of a water mediated hydrogen-bonding network that connects (+)-12 with both the outer domain (Asp368_{gp120}) and the bridging sheet (Met426_{gp120}). Thus, between the two complexes [(+)-12 versus (-)-12], a unique pattern of hydrogen bonding exists between the guanidinium moiety, ordered water molecules, and the gp120 outer and bridging sheet domains. As judged by the dissociation constant of

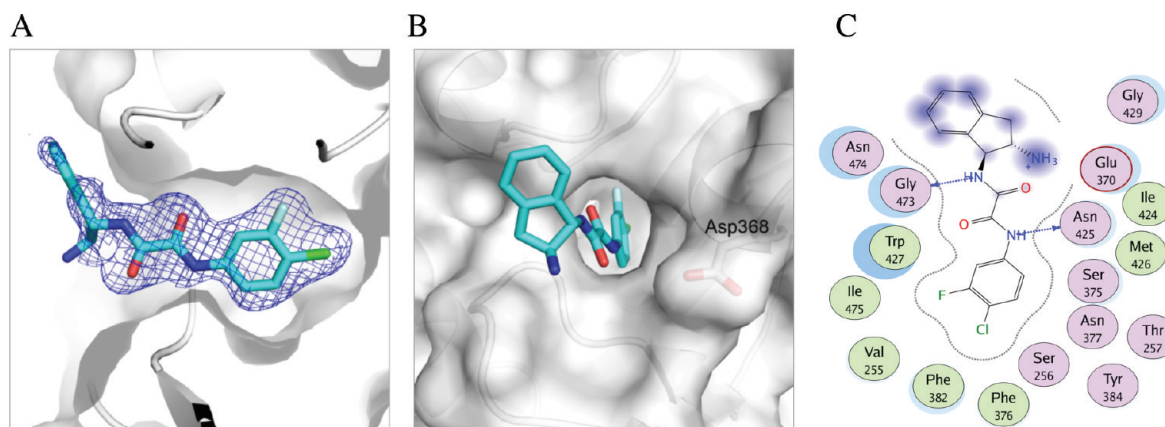


Figure 7. Crystal structure of (+)-6 bound to gp120: (A) $2F_o - F_c$ electron density map of (+)-6 bound within the Phe43 cavity of gp120_(H375S) core_c contoured at 1σ ; (B) position of (+)-6 region III relative to Asp368_{gp120}; (C) (+)-6–gp120–ligand interaction map, as described in Figure 1.

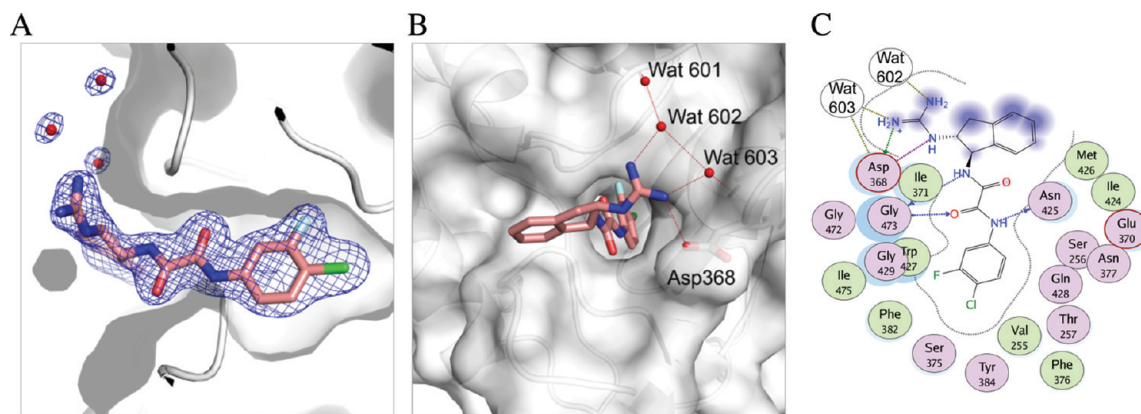


Figure 8. Crystal structure of (–)-12 bound to gp120: (A) $2F_o - F_c$ electron density map of (–)-12 (pink) and four crystallographic water molecules (red spheres) bound within the Phe43 cavity of gp120_(H375S) core_e contoured at 1.2 σ ; (B) position of (–)-12 region III relative to Asp368_{gp120} illustrating the water-mediated hydrogen bonding network; (C) (–)-12–gp120 ligand interaction map, as described in Figure 1.

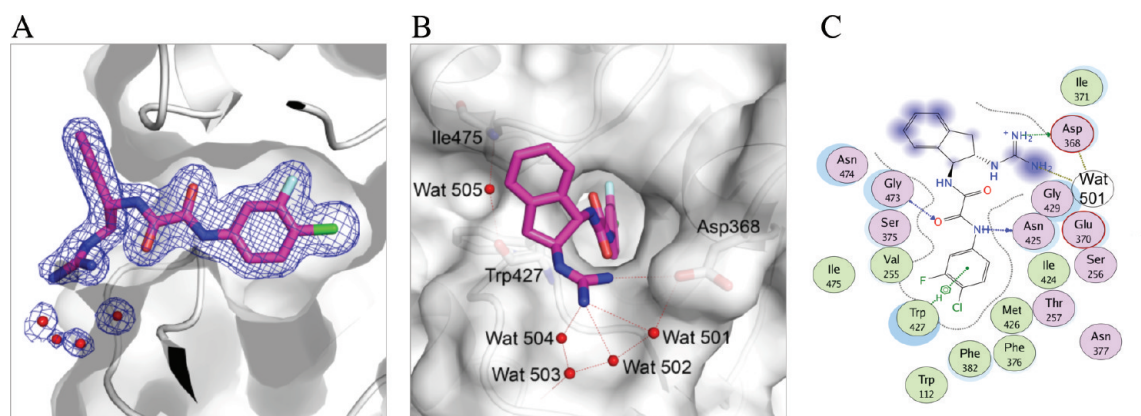


Figure 9. Crystal structure of (+)-12 bound to gp120: (A) $2F_o - F_c$ electron density map of (+)-12 (magenta) and four crystallographic water molecules (red spheres) bound within the Phe43 cavity of gp120_(H375S) core_e contoured at 1.2 σ ; (B) position of (+)-12 region III relative to Asp368_{gp120} illustrating the water-mediated hydrogen bonding network; (C) (+)-12–gp120 ligand interaction map, as described in Figure 1.

(+)-12 ($K_d = 0.25 \mu\text{M}$) and (–)-12 ($K_d = 0.30 \mu\text{M}$) compared to (+)-6 ($K_d = 1.9 \mu\text{M}$), the guanidinium–Asp368_{gp120} interaction and water mediated hydrogen bonding contributes favorably to the binding affinity of both (+)-12 and (–)-12 to gp120. Furthermore, the distinct thermodynamic signatures of gp120 binding between the (+)-12 and (–)-12 enantiomers are consistent with the different binding modes revealed in the crystal structures of these enantiomeric compounds bound to gp120.

CONCLUSIONS

We have targeted the highly conserved Phe43 cavity and Asp368_{gp120} hotspots at the protein–protein interface of the CD4–gp120 complex to improve the antiviral potency and breadth of 1–4. In this work a modified ROCS “scaffold hopping”,^{60,61} virtual screening strategy was employed to develop inhibitors that target both the Phe43_{gp120} and Asp368_{gp120} hotspots. A hypothetical 1,1-diamine molecule (5), encompassing the desired chemotype and spatial features, was employed to search chemical space to identify a lead compound possessing a basic amine directed toward the Asp368 hotspot. This strategy, in conjunction with molecular design and synthesis, has led to the identification of two novel analogues that employ the *trans*-1,2-disubstituted indane scaffold [e.g., (–)-12 and (+)-12] to direct a guanidinium group toward the Asp368_{gp120} hotspot.

We subsequently demonstrated that (–)-12 and (+)-12 specifically inhibit HIV-1 entry through interaction with the Env spike by virtue of the incorporation of a guanidinium group. Both (–)-12 and (+)-12 have improved and broad antiviral potency and, importantly, do not enhance viral infection in CD4-negative cells. The wide neutralization breadth against diverse strains of clades B and C viral isolates validates the importance of considering strain variability when evaluating binding hotspots appropriate for inhibitor design. Furthermore, in the context of CD4-negative cells, amines (–)-6 and (+)-6 function as agonists, promoting the CD4-independent viral entry process. Incorporation of the guanidinium functionality to afford (–)-12 and (+)-12 converts these agonists to antagonists of viral entry and eliminates the undesired property of promoting CD4-independent viral entry. The ability to suppress the undesired agonist properties demonstrates that the Phe43 cavity of gp120 and the NBD compound class remains an attractive target for the development of HIV-1 entry inhibitors.

The crystal structures described herein further confirm our design criteria and represent the highest resolution structures, to date, of a small molecule entry antagonist bound to the gp120 core. Importantly, the guanidinium groups of (–)-12 and (+)-12 form an electrostatic interaction with Asp368_{gp120} and reveal two distinct water-mediated hydrogen-bonding networks between the antagonist guanidinium group and

Asp368_{gp120}. Interestingly, (–)-12 and (+)-12 also display distinct thermodynamic signatures. The smaller unfavorable entropy for (+)-12 binding to gp120, along with the favorable binding efficiency and surface efficiency indices, may make this enantiomer a more suitable candidate for continued optimization. The modest IC₅₀ = 20 μ M exhibited by (–)-12 and (+)-12 indicates that additional optimization will be required to make this class of molecules more effective. In region I, the surface complementarity of the halogenated phenyl ring could be improved, and in region III, the guaninidium–Asp368_{gp120} interactions could be strengthened and the adjacent bound solvent incorporated in compound design. Therefore, the high-resolution crystal structures of these antagonists, with demonstrated improvement in antiviral potency and breadth, provide a novel structural paradigm to facilitate future cycles of design, synthesis, and biological evaluation to develop this class of small molecule inhibitors of HIV-1 entry.

EXPERIMENTAL SECTION

Small Molecule Modeling. Molecules were constructed in MOE⁷³ and ionized using MOE's WashMDB function, and hydrogens were added. The small molecule conformation was minimized to a gradient of 0.01 with the MMFF94x^{74,75} using a distance-dependent dielectric constant of 1.

Protein Modeling. Molprobit^{76,77} was used to add hydrogen atoms and determine the tautomeric states and orientation of Asn, Gln, and His in the X-ray crystal structure of 4 bound to HIV-1 clade A/E gp120_(H375S) core_e. Hydrogens were added to crystallographic waters using MOE (2010).⁷³ The OPSLAA⁷⁸ force field in MOE was used, and all hydrogen atoms were minimized to an rms gradient of 0.01, holding the remaining heavy atoms fixed. A stepwise minimization followed for all atoms, using a quadratic force constant (100) to tether the atoms to their starting geometries. For each subsequent minimization, the force constant was reduced by a half until 0.25. This was followed by a final cycle of unrestrained minimization.

Docking. GOLD (version 4.0.1)^{57,58} was used for docking, and the binding site was defined by using the crystallographic position of 4. One-hundred genetic algorithm (GA) docking runs were performed with the following parameters: initial_virtual_pt_match_max=3.5, diverse_solutions=1, divsol_cluster_size=1, and divsol_rmsd=1.5. All other parameters were set to defaults.

ROCS Virtual Screening. Flipper from Open Eye was used to expand compounds with unspecified chirality prior to generation of conformers. Using Omega (version 2.2.1)⁷⁹ from Open Eye with default parameters, a maximum of 50 low energy conformers for all compounds in the ZINC database (version 7)⁶² were generated and stored in sd files of approximately 10 000 molecules. ROCS^{60,61} searches were run using 3D coordinates from the docked binding mode of the amine containing the tetramethylpiperidine prototype. The implicit Mills–Dean⁸⁰ force field was used to match chemotypes as well as shape. Hits were ranked by a combination of the Tanimoto coefficient and the scaled color score (ComboScore). Primary amines with ComboScore > 1.0 were selected from the set of hits, filtered for currently commercial availability, and conjugated in silico and were docked with GOLD^{57,58} and scored with a mass-corrected Goldscore.

Synthesis Procedures. All reactions were conducted in oven-dried glassware under an inert atmosphere of nitrogen or argon unless otherwise stated. All solvents were reagent or high performance liquid chromatography (HPLC) grade. Anhydrous CH₂Cl₂ and THF were obtained from the Pure Solve PS-400 system under an argon atmosphere. All reagents were purchased from commercially available sources and used as received. Mixtures were magnetically stirred under a nitrogen atmosphere and reactions monitored by either thin layer chromatography (TLC) with 0.25 mm E. Merck precoated silica gel plates or analytical HPLC. Yields refer to chromatographically and spectroscopically pure compounds. Optical rotations were measured on a JASCO P-2000 polarimeter within the specified solvent. Proton

and carbon-13 NMR spectra were recorded on a Bruker AM-500 at 305 K unless otherwise noted. Chemical shifts are reported relative to chloroform (δ 7.26), methanol (δ 3.31), or dimethyl sulfoxide (δ 2.50) for ¹H NMR and chloroform (δ 77.0), methanol (δ 49.2), or dimethyl sulfoxide (δ 39.4) for ¹³C NMR. High-resolution mass spectra were recorded at the University of Pennsylvania Mass Spectroscopy Service Center on either a VG Micromass 70/70H or VG ZAB-E spectrometer. Analytical HPLC was performed with a Waters HPLC–MS system, consisting of a 515 pump and Sunfire C18 reverse phase column (20 μ L injection volume, 5 μ m packing material, 4.5 mm \times 50 mm column dimensions) with detection accomplished by a Micromass ZQ mass spectrometer and 2996 photodiode array detector. Preparative HPLC was performed with a Gilson 333/334 preparative pump system equipped with a 5 mL injection loop, Sunfire C18 OBD column (5 μ m packing material, 19 mm \times 100 mm column dimensions) equipped with a UV–vis dual wavelength detector (210 and 254 nm) and 215 liquid handling module. Solvent systems employed were based on the following buffers: buffer A consisting of H₂O containing 0.05% formic acid; buffer B consisting of MeCN containing 0.05% formic acid. The purity of new compounds was judged by NMR and HPLC–MS to be in excess of 95%.

N¹-(4-Chloro-3-fluorophenyl)-N²-[(1S,2R)-2-hydroxy-2,3-dihydro-1H-inden-1-yl]oxalamide [(+)-9]. To a solution containing ethyl 2-(4-chloro-3-fluorophenylamino)-2-oxoacetate (7) (1.87 g, 7.62 mmol) in 20 mL of EtOH was added (1S,2R)-1-amino-2,3-dihydro-1H-inden-2-ol [(–)-8, 1.19 g, 7.98 mmol] in one portion. The reaction mixture was stirred and heated to 150 °C in a sealed tube for 1 h, after which the suspension was allowed to cool to room temperature. The precipitate was collected by vacuum filtration and washed with small portions of dichloromethane to provide 2.22 g (83%) of analytically pure TK-II-52 (+)-9 as a white semicrystalline solid. [α]_D²⁵ +103.5° (c 0.56, DMSO); ¹H NMR (500 MHz, DMSO-*d*₆) δ 11.19 (s, 1H), 8.36 (d, *J* = 8.7 Hz, 1H), 7.97, (dd, *J* = 2, 11.7 Hz, 1H), 7.77, (d, *J* = 8.8 Hz, 1H), 7.59, (t, *J* = 8.7 Hz, 1H), 7.28–7.18, (m, 4H), 5.46, (d, *J* = 4.9 Hz, 1H), 5.25, (dd, *J* = 5.2, 8.6 Hz, 1H), 4.52, (dd, *J* = 4.6, 8.6 Hz, 1H), 3.14, (dd, *J* = 4.9, 16.2 Hz, 1H), 2.88, (d, *J* = 16.1 Hz, 1H); ¹³C NMR (125 MHz, DMSO-*d*₆) δ 159.3, 158.8, 156.8, (d, *J*_{CF} = 242.5 Hz), 141.0, 140.8, 138.2, (d, *J*_{CF} = 10 Hz), 131.6, 127.7, 126.5, 125.0, 124.1, 117.5 (d, *J*_{CF} = 2.9 Hz), 114.5 (d, *J*_{CF} = 17.5 Hz), 108.6, (d, *J*_{CF} = 25 Hz), 71.6, 56.9. HRMS (ES⁺) *m/z* 371.0572 [(M + Na)⁺; calcd for C₁₇H₁₄ClFN₂O₃, 371.0575].

N¹-(4-Chloro-3-fluorophenyl)-N²-[(1S,2S)-2-azido-2,3-dihydro-1H-inden-1-yl]oxalamide [(+)-10]. To a solution containing (+)-9 (2.20 g, 6.31 mmol) in a mixture of dichloroethane (50 mL) and THF (10 mL) was added *p*-toluenesulfonyl chloride (3.60 g, 18.88 mmol), followed by NEt₃ (2.64 mL, 18.91 mmol), DMAP (0.77 g, 2.82 mmol), and a stir bar. A reflux condenser was attached, and the solution was heated to 60 °C and stirred for 2 h. After cooling, the reaction mixture was quenched with 100 mL of saturated NH₄Cl solution, followed by extraction with DCM/EtOAc (3:1, 3 \times 100 mL). The combined organic fractions were washed with brine and dried over Na₂SO₄, filtered, and concentrated in vacuo. The crude product was sonicated in 50 mL of DCM/hexanes (1:1) for 30 min and then filtered. The filtrate was then washed with DCM/hexanes (1:1, 2 \times 25 mL) to provide 2.21 g (70%) of the desired tosylate [(+)-SI-1] as a white flakey solid. [α]_D²⁵ +10.4° (c 0.29, CH₂Cl₂); ¹H NMR (500 MHz, DMSO-*d*₆) δ 10.97 (s), 8.84 (d, *J* = 9.0 Hz, 1H), 8.00 (dd, *J* = 2.5, 12.0 Hz, 1H), 7.79 (dd, *J* = 2.0, 9.0 Hz, 1H), 7.75 (d, *J* = 8 Hz, 2H), 7.62 (t, *J* = 8.5 Hz, 1H), 7.33–7.22 (m, 6H), 5.49 (dd, *J* = 5.0, 8.5 Hz, 1H), 5.24 (dt, *J* = 1.5, 5.0 Hz, 1H), 3.34 (m, overlap with water, 1H), 3.13 (d, *J* = 16.0 Hz, 1H), 2.33 (s, 3H); ¹³C NMR (125 MHz, DMSO-*d*₆) δ 159.4, 157.9, 156.8 (d, *J*_{CF} = 243.8 Hz), 144.8, 138.7, 138.6, 138.2, (d, *J*_{CF} = 10 Hz), 132.7, 130.6, 129.9, 128.3, 127.5, 127.0, 124.8, 123.9, 117.3, (d, *J*_{CF} = 2.7 Hz), 114.4, (d, *J*_{CF} = 17.5 Hz), 108.4, (d, *J*_{CF} = 25.0 Hz), 82.7, 55.6, 37.6, 20.9. HRMS (ES⁺) *m/z* 503.0862 [(M + H)⁺; calcd for C₂₄H₂₀ClFN₂O₅S, 503.0844].

To a solution of (+)-SI-1 (2.20 g, 4.38 mmol), prepared above, in 8 mL of DMSO were added NaN₃ (2.86 g, 43.99 mmol) and a stir bar. The solution was heated to 50 °C and stirred for 2.5 h. After the mixture was cooled to room temperature, the reaction was quenched

with H₂O (50 mL) followed by extraction with DCM/EtOAc (3:1, 3 × 100 mL). The combined organic fractions were washed with brine (3 × 100 mL), dried over Na₂SO₄, filtered, and concentrated in vacuo. The crude product was then dissolved in a minimal amount of hot EtOAc, followed by addition of an equal portion of hot hexane. The obtained precipitate was collected, the mother liquor concentrated, and the residual solid recrystallized via the same procedure. The isolated solids were combined to provide 1.30 g (79%) of the azide (+)-**10** as a white flakey solid. $[\alpha]_D^{25} +40.7^\circ$ (c 0.51, EtOAc); ¹H NMR (500 MHz, DMSO-*d*₆) δ 11.14 (s, 1H), 9.66 (d, *J* = 9.0 Hz, 1H), 7.98 (dd, *J* = 2.0, 11.5 Hz, 1H), 7.77 (dd, *J* = 1.5, 8.5 Hz, 1H), 7.60 (t, *J* = 8.5 Hz, 1H), 7.28–7.22 (m, 3H), 7.15 (d, *J* = 7.0 Hz, 1H), 5.34 (t, *J* = 8.0 Hz, 1H), 4.54 (q, *J* = 8.0 Hz, 1H), 3.34 (dd, *J* = 7.5, 15.5 Hz, 1H), 2.88 (dd, *J* = 8.5, 15.5 Hz, 1H); ¹³C NMR (125 MHz, DMSO-*d*₆) δ 160.1, 158.5, 156.8, (d, *J*_{CF} = 242.5 Hz), 139.9, 138.8, 138.2 (d, *J*_{CF} = 10 Hz), 130.5, 128.2, 127.1, 124.7, 123.4, 117.4, (d, *J*_{CF} = 3.0 Hz), 114.4, (d, *J*_{CF} = 17.8 Hz), 108.5, (d, *J*_{CF} = 25.6 Hz), 65.7, 59.4, 35.3. HRMS (ES+) *m/z* 372.0652 [(M – H)[–]; calcd for C₁₇H₁₂ClFN₃O₂, 372.0664].

N¹-(4-Chloro-3-fluorophenyl)-N²-[(1S,2S)-2-amino-2,3-dihydro-1H-inden-1-yl]oxalamide [AWS-I-50, (+)-6**].** To a solution of (+)-**10** (1.30 g, 3.48 mmol) in 35 mL of MeOH were added Lindlar's catalyst (5% Pd/CaCO₃, poisoned with lead, 650 mg) and a stir bar. Hydrogen was bubbled through the solution, after which the reaction mixture was stirred for 2 h under a hydrogen atmosphere at room temperature. The reaction mixture was then filtered through a plug of Celite and the filter cake washed with additional methanol. The filtrate was concentrated in vacuo to obtain the crude product, which was then purified by silica gel chromatography utilizing a gradient solvent system (DCM/MeOH/NH₄OH, 100:1:0.1 to 50:1:0.1 to 20:1:0.1 to 10:1:0.1) to afford 1.06 g (87%) of amine (+)-**6** as a white flakey solid. $[\alpha]_D^{25} +93.0^\circ$ (c 0.14, MeOH); ¹H NMR (500 MHz, CDCl₃): δ 11.07 (s, 1H), 9.22 (d, *J* = 9.0 Hz, 1H), 7.98 (dd, *J* = 2.4, 11.9 Hz, 1H), 7.77 (ddd, *J* = 1.0, 2.5, 8.9 Hz, 1H), 7.60 (t, *J* = 8.7 Hz, 1H), 7.20–7.14 (m, 3H), 7.06 (d, *J* = 7.2 Hz, 1H), 5.00 (t, *J* = 8.5 Hz, 1H), 3.69 (q, *J* = 8.5 Hz, 1H), 3.08 (dd, *J* = 7.5 Hz, 1H), 2.64 (dd, *J* = 9.2 Hz, 1H); ¹³C NMR (125 MHz, DMSO-*d*₆) δ 160.3, 159.0, 156.8, (d, *J*_{CF} = 242.5 Hz), 142.0, 140.6, 138.3 (d, *J*_{CF} = 10 Hz), 130.6, 127.4, 126.4, 124.4, 123.3, 117.3, (d, *J*_{CF} = 3.75 Hz), 114.2, (d, *J*_{CF} = 17.5 Hz), 108.4 (d, *J*_{CF} = 25 Hz), 62.6, 59.6, 48.6. HRMS (ES+) *m/z* 348.0911 [(M + H)⁺; calcd for C₁₇H₁₅ClFN₃O₂, 348.0915].

N¹-(4-Chloro-3-fluorophenyl)-N²-[(1S,2S)-2-guanidino-2,3-dihydro-1H-inden-1-yl]oxalamide Formate [DMJ-I-228, (+)-12**].** To a solution containing (+)-**6** (1.06 g, 3.05 mmol) in 35 mL of DMF were added 1H-pyrazole-1-carboxamide hydrochloride (**11**, 879 mg, 6.00 mmol), *N,N*-diisopropylethylamine (2.10 mL, 12.06 mmol), and a stir bar. The solution was heated to 110 °C for 16 h and then allowed to cool. The light-red reaction mixture was concentrated to approximately 5 mL and diluted with 20 mL MeCN/H₂O (1:1), and the solution was subjected to purification via HPLC to give 350 mg (27%) of (+)-**12** as a white fluffy solid after lyophilization. $[\alpha]_D^{26} +5.8^\circ$ (c 0.72, MeOH); ¹H NMR (500 MHz, CD₃OD): δ 8.3 (br s, 1H_{formate}), 7.84 (dd, *J* = 2.5, 11.5 Hz, 1H), 7.50 (d, *J* = 8.75 Hz, 1H), 7.43 (t, *J* = 8.5 Hz, 1H), 7.34–7.29 (m, 4 H), 5.27 (d, *J* = 4.5 Hz, 1H), 4.30 (m, 1H), 3.52 (dd, *J* = 7.5 Hz, 1H), 2.93 (dd, *J* = 5, 16.5 Hz, 1H); ¹³C NMR (125 MHz, CD₃OD) δ 162.8, 159.4, 159.3, (d, *J*_{CF} = 244.4 Hz), 159.0, 141.9, 139.7, 139.1 (d, *J*_{CF} = 9.8 Hz), 131.9, 130.6, 129.0, 126.4, 126.3, 118.3 (d, *J*_{CF} = 3.3 Hz), 117.4 (d, *J*_{CF} = 17.8 Hz), 110.0 (d, *J*_{CF} = 26.3 Hz), 62.3, 59.7, 37.8. HRMS (ES+) *m/z* 390.1132 [(M + H)⁺; calcd for C₁₈H₁₈ClFN₃O₂, 390.1133]. The formate counterion was not observed under the HRMS conditions.

The enantiomeric compounds (–)-**6** and (–)-**12** were prepared using the procedures described above, starting with commercially available aminoindanol (+)-**8**. The intermediates and final compounds possess identical ¹H and ¹³C NMR spectra and HRMS data. The observed optical rotations were the following: (–)-**9**, $[\alpha]_D^{29} -112.1^\circ$ (c 0.48, DMSO); (–)-**10**, $[\alpha]_D^{25} -34.9^\circ$ (c 0.30, EtOAc); (–)-**6**, $[\alpha]_D^{25} -83.2^\circ$ (c 0.16, MeOH); (–)-**12**, $[\alpha]_D^{25} -3.2^\circ$ (c 0.72, MeOH).

Cell-Based Infectivity Assays: General Considerations. Compounds were dissolved in dimethyl sulfoxide (DMSO) and

stored at 10 mM at –20 °C. The compounds were diluted in Dulbecco's modified Eagle medium (DMEM, Invitrogen) to create 1 mM solutions before use. Soluble CD4 (sCD4) was purchased from ImmunoDiagnostics (Woburn, MA). Human 293T embryonic kidney and canine Cf2Th thymocytes (ATCC) were grown at 37 °C and 5% CO₂ in DMEM (Invitrogen) containing 10% fetal bovine serum (Sigma) and 100 µg/mL penicillin–streptomycin (Mediatech, Inc.). Cf2Th cells stably expressing human CD4 and either CCR5 or CXCR4^{81,82} were grown in medium supplemented with 0.4 mg/mL G418 (Invitrogen) and 0.20 mg/mL hygromycin B (Roche Diagnostics). By use of the Effectene transfection reagent (Qiagen), 293T human embryonic kidney cells were co-transfected with plasmids expressing the pCMVΔP1ΔenvpA HIV-1 Gag-Pol packaging construct, the wild-type or mutant HIV-1_{YU2} envelope glycoproteins or the envelope glycoproteins of the control amphotropic murine leukemia virus (A-MLV), and the firefly luciferase-expressing vector at a DNA ratio of 1:1:3 µg. For the production of viruses pseudotyped with the A-MLV glycoprotein, a *rev*-expressing plasmid was added. The single-round, replication-defective viruses in the supernatants were harvested 24–30 h after transfection, filtered (0.45 µm), aliquoted, and frozen at –80 °C until further use. The reverse transcriptase (RT) activities of all viruses were measured as described previously.⁸³

Assay of Virus Infectivity and Inhibitor Sensitivity. Cf2Th/CD4-CCR5 or Cf2Th/CD4-CXCR4 target cells were seeded at a density of 6 × 10⁵ cells/well in 96-well luminometer-compatible tissue culture plates (Perkin-Elmer) 24 h before infection. On the day of infection, 1–100 µM was added to recombinant viruses (10 000 reverse transcriptase units) in a final volume of 50 µL and incubated at 37 °C for 30 min. The medium was removed from the target cells, which were then incubated with the virus–drug mixture for 2–4 h at 37 °C. At the end of this time point, complete medium was added to a final volume of 150 µL and incubated for 48 h at 37 °C. The medium was removed from each well, and the cells were lysed with 30 µL of passive lysis buffer (Promega) by three freeze–thaw cycles. An EG&G Berthold microplate luminometer LB 96V was used to measure luciferase activity in each well after the addition of 100 µL of luciferin buffer (15 mM MgSO₄, 15 mM potassium phosphate buffer [pH 7.8], 1 mM ATP, 1 mM dithiothreitol) and 50 µL of 1 mM D-luciferin potassium salt (BD Pharmingen).

Luminescent Cell-Based Viability Assay. Compounds were dissolved in dimethyl sulfoxide (DMSO) and stored at 10 mM at –20 °C. The compounds were diluted in Dulbecco's modified Eagle medium (DMEM, Invitrogen) to create 1 mM solutions before use. In addition, DMSO (Sigma) was also diluted in DMEM and used as negative control. Cytotoxicity assay was done in parallel with the cell-based infection assay as described in the methods section of this article using Cf2Th cells stably expressing human CD4 and CCR5. Briefly, Cf2Th/CD4-CCR5 target cells were seeded at a density of 6 × 10⁵ cells/well in 96-well luminometer-compatible tissue culture plates (Perkin-Elmer) 24 h before infection. On the day of infection, medium from target cells was removed and 1–100 µM (+)-**12** or DMSO to 2% (equivalent to concentration of DMSO in 100 µM (+)-**12**) was added to target cells at a final volume of 50 µL and incubated at 37 °C for 2–4 h. At the end of this time point, complete medium was added to a final volume of 150 µL and incubated for 48 h at 37 °C. After 48 h, the plates were equilibrated to room temperature for 30 min and 30 µL of substrate reagent, CellTiter-Glo (Promega), was added to each well and incubated at room temperature for 5–10 min. An EG&G Berthold microplate luminometer LB 96V was used to measure luciferase activity in each well for 5 s.

Isothermal Titration Calorimetry. Isothermal titration calorimetric experiments were performed using a high-precision VP-ITC titration calorimetric system from MicroCal LLC (Northampton, MA). The calorimetric cell (~1.4 mL), containing gp120 at about 2 µM dissolved in PBS, pH 7.4 (Roche Diagnostics GmbH), with 2% DMSO, was titrated with the different compounds dissolved in the same buffer at 80–130 µM. The compound solution was added in aliquots of 10 µL at preset intervals. All solutions were degassed to avoid any formation of bubbles in the calorimeter during stirring. All experiments were performed at 25 °C. The heat evolved upon

injection of compound was obtained from the integral of the calorimetric signal. The heat associated with the binding reaction was obtained by subtracting the heat of dilution from the heat of reaction. The individual binding heats were plotted against the molar ratio, and the values for the enthalpy change (ΔH) and association constant, K_a ($K_d = 1/K_a$), were obtained by nonlinear regression of the data.

Viral Breadth Studies. HIV-1 Env-pseudoviruses were prepared by transfecting 293T cells with 10 μg of rev/Env expression plasmid and 30 μg of an Env-deficient HIV-1 backbone vector (pSG3 Δenv), using FuGENE 6 transfection reagents (Invitrogen). Pseudovirus-containing culture supernatants were harvested 2 days after transfection, filtered (0.45 μm), and stored at -80°C or in the vapor phase of liquid nitrogen. Neutralization was measured using HIV-1 Env-pseudoviruses to infect TZM-bl cells as described previously^{84–87} with minor modifications. Briefly, the test reagent [(+)-12, (–)-12, 1, or CD4-Ig] was diluted in complete medium containing 10% DMSO. Then 40 μL of virus was added to 10 μL of serially diluted test reagent in duplicate wells of a 96-well flat bottom culture plate, and the virus–reagent mix was incubated for 30 min at 37°C . To keep assay conditions constant, sham medium containing 10% DMSO was used in place of test reagent in specified control wells. The virus input was set at a multiplicity of infection of approximately 0.01–0.1, which generally results in 100000–400000 relative light units (RLUs) in a luciferase assay (Promega, Madison, WI). The test reagent concentrations were defined at the point of incubation with virus supernatant. Neutralization curves were fit by nonlinear regression using a five-parameter Hill slope equation as previously described.⁸⁶ The 50% or 80% inhibitory concentrations (IC_{50} or IC_{80}) were reported as the reagent concentrations required to inhibit infection by 50% or 80%.

Construction of the HIV-1 Envelope Sequence Phylogenetic Trees. The HIV-1 gp160 protein sequences of isolates used in the neutralization assays were aligned using MUSCLE (multiple sequence comparison by log expectation).^{88,89} The protein distance matrix was calculated by “protdist” using the Jones–Taylor–Thornton model,⁹⁰ and the dendrogram was constructed using the neighbor-joining method⁹¹ by “Neighbor”. The analysis was performed at the NIAID Biocluster (<https://niaid-biocluster.niaid.nih.gov/>). The trees were displayed with Dendroscope.⁹²

Plasmids. A point mutation was introduced to pVRC8400-HIV-1 clade A/E_{93TH057} ΔV123 expression vector to generate clade A/E_{93TH057} gp120 core_e (H375S) expressing plasmid. The plasmid construct was verified by DNA sequencing.

Crystallization, Data Collection, Structure Determination, and Refinement. Clade A/E_{93TH057} gp120_(H375S) core_e was purified as described.³⁴ Small molecules in 100% DMSO were incorporated in the purified gp120 to make a final concentration of 100 μM . Then the small molecule–gp120 complexes were set up for crystallization using vapor diffusion at 20°C . Crystals grew in a mixture of 0.5 μL of protein–small molecule complex and 0.5 μL of reservoir solution containing 8–10% (v/v) PEG 8000, 5% isopropanol, 0.1 M HEPES (pH 7.5). Crystals were soaked in cryoprotection solution containing 30% ethylene glycol, 12% PEG 8000, and 0.1 M HEPES (pH 7.5) and were flash frozen in liquid nitrogen. Data were collected on beamline SERCAT ID-22 at the Advanced Photon Source and processed with HKL2000.⁹³ The structures were solved by molecular replacement with PHENIX⁹⁴ using the coordinates of unliganded clade A/E_{93TH057} gp120 core_e (PDB code 3TGT). The initial $F_o - F_c$ map generated after a rigid body refinement clearly indicated the electron densities of (–)-12 and (+)-12 and allowed us to place them into the densities manually using COOT.⁹⁵ The initial densities of 4 and (+)-6, however, were not as clear as those found in (–)-12 and (+)-12, specifically in the region III. After several rounds of refinement using PHENIX,⁹⁴ the $R_{\text{work}}/R_{\text{free}}$ values for (–)-12 and (+)-12 converged to 18.8/20.8% and 19.3/23.3%, respectively (Table 3). The geometry of the refined model was checked with Molprobity.⁹⁶ Figures 1, 2, and 7–9 were generated by PyMOL.⁹⁷ To facilitate analysis of protein–ligand interactions in the context of the crystal structures, hydrogen atoms

were added to all atoms within a 4.5 Å radius of the small molecule ligand and were minimized in the Merck molecular force field.^{74,75}

■ ASSOCIATED CONTENT

Supporting Information

SPR, mutation, and neutralization data and NMR spectra. This material is available free of charge via the Internet at <http://pubs.acs.org>.

Accession Codes

Coordinates and structure factors have been deposited in the Protein Data Bank with the following accession numbers: 4DKO, 4DKP, 4DKQ, and 4DKR.

■ AUTHOR INFORMATION

Corresponding Author

*For J.M.L.: phone, 610-526-5679; e-mail, jlalonde@brynmaur.edu. For A.B.S.: phone, 215-898-4860; e-mail, smithab@sas.upenn.edu.

Author Contributions

[∞]These authors contributed equally to this work.

Notes

The authors declare no competing financial interest.

■ ACKNOWLEDGMENTS

We thank Irwin Chaiken and Wayne Hendrickson and all the members of the PO1 Consortium “Structure-Based Antagonism of HIV-1 Envelope Function in Cell Entry”. We also thank Jonathan Stuckey for assistance with figures, and members of the Structural Biology Section, Vaccine Research Center, NIAID for comments on the manuscript. Funding was provided by NIH Grant GM 56550 to J.M.L., E.F., A.B.S., by NIH Intramural IATAP and NIAID programs to Y.D.K., P.D.K., J.R.M., and J.S. J.M.L. thanks the Pittsburgh Supercomputing Center for an allocation for computing resources, Grant MCB090108.

■ ABBREVIATIONS USED

HIV-1, human immunodeficiency virus type 1; SIV, simian immunodeficiency virus; sCD4, soluble CD4; ITC, isothermal titration calorimetry; A-MLV, amphotropic murine leukemia virus; GMT, geometric mean titer; SPR, surface plasmon resonance; BEI, binding efficiency index; SEI, surface efficiency index; GA, genetic algorithm; HRMS, high-resolution mass spectrometry; DMEM, Dulbecco's modified Eagle medium; TsCl, tosyl chloride; DMAP, 4-dimethylaminopyridine

■ REFERENCES

- (1) Barre-Sinoussi, F.; Chermann, J. C.; Rey, F.; Nugeyre, M. T.; Chamaret, S.; Gruest, J.; Dauguet, C.; Axler-Blin, C.; Vezinet-Brun, F.; Rouzioux, C.; Rozenbaum, W.; Montagnier, L. Isolation of a T-lymphotropic retrovirus from a patient at risk for acquired immune deficiency syndrome (AIDS). *Science* **1983**, *220*, 868–871.
- (2) Gallo, R. C.; Salahuddin, S. Z.; Popovic, M.; Shearer, G. M.; Kaplan, M.; Haynes, B. F.; Palker, T. J.; Redfield, R.; Oleske, J.; Safai, B.; et al. Frequent detection and isolation of cytopathic retroviruses (HTLV-III) from patients with AIDS and at risk for AIDS. *Science* **1984**, *224*, 500–503.
- (3) Dalgleish, A. G.; Beverley, P. C.; Clapham, P. R.; Crawford, D. H.; Greaves, M. F.; Weiss, R. A. The CD4 (T4) antigen is an essential component of the receptor for the AIDS retrovirus. *Nature* **1984**, *312*, 763–767.
- (4) McDougal, J. S.; Kennedy, M. S.; Sligh, J. M.; Cort, S. P.; Mawle, A.; Nicholson, J. K. Binding of HTLV-III/LAV to T4+ T cells by a

complex of the 110K viral protein and the T4 molecule. *Science* **1986**, 231.

(5) Klatzmann, D.; Champagne, E.; Chamaret, S.; Gruest, J.; Guetard, D.; Hercend, T.; Gluckman, J. C.; Montagnier, L. T-lymphocyte T4 molecule behaves as the receptor for human retrovirus LAV. *Nature* **1984**, 314, 767–768.

(6) Wyatt, R.; Sodroski, J. The HIV-1 envelope glycoproteins fusogens antigens and immunogens. *Science* **1998**, 280, 1884–1888.

(7) Ugolini, S.; Moulard, M.; Mondor, I.; Barois, N.; Demandolx, D.; Hoxie, J.; Brelot, A.; Alizon, M.; Davoust, J.; Sattentau, Q. J. HIV-1 gp120 induces an association between CD4 and the chemokine receptor CXCR4. *J. Immunol.* **1997**, 159, 3000–3008.

(8) Blacklow, S. C.; Lu, M.; Kim, P. S. A trimeric subdomain of the simian immunodeficiency virus envelope glycoprotein. *Biochemistry* **1995**, 34, 14955–14962.

(9) Lu, M.; Blacklow, S. C.; Kim, P. S. A trimeric structural domain of the HIV-1 transmembrane glycoprotein. *Nat. Struct. Biol.* **1995**, 2, 1075–1082.

(10) Kowalski, M.; Potz, J.; Basiripour, L.; Dorfman, T.; Goh, W. C.; Terwilliger, E.; Dayton, A.; Rosen, C.; Haseltine, W.; Sodroski, J. Functional regions of the envelope glycoprotein of human immunodeficiency virus type 1. *Science* **1987**, 237, 1351–1355.

(11) Sattentau, Q. J.; Moore, J. P. Conformational changes induced in the human immunodeficiency virus envelope glycoprotein by soluble CD4 binding. *J. Exp. Med.* **1991**, 174, 407–415.

(12) Sattentau, Q. J.; Moore, J. P.; Vignaux, F.; Traincard, F.; Poignard, P. Conformational changes induced in the envelope glycoproteins of the human and simian immunodeficiency viruses by soluble receptor binding. *J. Virol.* **1993**, 67, 7383–7393.

(13) Wu, H.; Myszk, D. G.; Tendian, S. W.; Brouillette, C. G.; Sweet, R. W.; Chaiken, I. M.; Hendrickson, W. A. Kinetic and structural analysis of mutant CD4 receptors that are defective in HIV gp120 binding. *Proc. Natl. Acad. Sci. U.S.A.* **1996**, 93, 15030–15035.

(14) Dragic, T.; Litwin, V.; Allaway, G. P.; Martin, S. R.; Huang, Y.; Nagashima, K. A.; Cavanaugh, C.; Maddon, P. J.; Koup, R. A.; Moore, J. P.; Paxton, W. A. HIV-1 entry into CD4+ cells is mediated by the chemokine receptor CC-CKR-5. *Nature* **1996**, 381, 667–673.

(15) Choe, H.; Farzan, M.; Sun, Y.; Sullivan, N.; Rollins, B.; Ponath, P. D.; Wu, L.; Mackay, C. R.; LaRosa, G.; Newman, W.; Gerard, N.; Gerard, C.; Sodroski, J. The beta-chemokine receptors CCR3 and CCR5 facilitate infection by primary HIV-1 isolates. *Cell* **1996**, 85, 1135–1148.

(16) Deng, H.; Liu, R.; Ellmeier, W.; Choe, S.; Unutmaz, D.; Burkhart, M.; Di Marzio, P.; Marmon, S.; Sutton, R. E.; Hill, C. M.; Davis, C. B.; Peiper, S. C.; Schall, T. J.; Littman, D. R.; Landau, N. R. Identification of a major co-receptor for primary isolates of HIV-1. *Nature* **1996**, 381, 661–666.

(17) Doranz, B. J.; Rucker, J.; Yi, Y.; Smyth, R. J.; Samson, M.; Peiper, S. C.; Parmentier, M.; Collman, R. G.; Doms, R. W. A dual-tropic primary HIV-1 isolate that uses fusin and the beta-chemokine receptors CKR-5, CKR-3, and CKR-2b as fusion cofactors. *Cell* **1996**, 85, 1149–1158.

(18) Bosch, M. L.; Earl, P. L.; Fargnoli, K.; Picciafuoco, S.; Giombini, F.; Wong-Staal, F.; Franchini, G. Identification of the fusion peptide of primate immunodeficiency viruses. *Science* **1989**, 244, 694–697.

(19) Brasseur, R.; Cornet, B.; Burny, A.; Vandenbranden, M.; Ruyschaert, J. M. Mode of insertion into a lipid membrane of the N-terminal HIV gp41 peptide segment. *AIDS Res. Hum. Retroviruses* **1988**, 4, 83–90.

(20) Helseth, E.; Olshevsky, U.; Gabuzda, D.; Ardman, B.; Haseltine, W.; Sodroski, J. Changes in the transmembrane region of the human immunodeficiency virus type 1 gp41 envelope glycoprotein affect membrane fusion. *J. Virol.* **1990**, 64, 6314–6318.

(21) Dorr, P.; Westby, M.; Dobbs, S.; Griffin, P.; Irvine, B.; Macartney, M.; Mori, J.; Rickett, G.; Smith-Burchnell, C.; Napier, C.; Webster, R.; Armour, D.; Price, D.; Stammen, B.; Wood, A.; Perros, M. Maraviroc (UK-427,857), a potent, orally bioavailable, and selective small-molecule inhibitor of chemokine receptor CCR5 with broad-

spectrum anti-human immunodeficiency virus type 1 activity. *Antimicrob. Agents Chemother.* **2005**, 49, 4721–4732.

(22) Kilby, J. M.; Hopkins, S.; Venetta, T. M.; DiMassimo, B.; Cloud, G. A.; Lee, J. Y.; Alldredge, L.; Hunter, E.; Lambert, D.; Bolognesi, D.; Matthews, T.; Johnson, M. R.; Nowak, M. A.; Shaw, G. M.; Saag, M. S. Potent suppression of HIV-1 replication in humans by T-20, a peptide inhibitor of gp41 mediated virus entry. *Nat. Med.* **1998**, 4, 1302–1307.

(23) Teixeira, C.; Gomes, J. R.; Gomes, P.; Maurel, F.; Barbault, F. Viral surface glycoproteins, gp120 and gp41, as potential drug targets against HIV-1: brief overview one quarter of a century past the approval of zidovudine, the first anti-retroviral drug. *Eur. J. Med. Chem.* **2011**, 46, 979–992.

(24) Zhan, P.; Li, W.; Chen, H.; Liu, X. Targeting protein–protein interactions: a promising avenue of anti-HIV drug discovery. *Curr. Med. Chem.* **2010**, 17, 3393–3409.

(25) Kadow, J.; Wang, H. G.; Lin, P. F. Small-molecule HIV-1 gp120 inhibitors to prevent HIV-1 entry: an emerging opportunity for drug development. *Curr. Opin. Invest. Drugs* **2006**, 7, 721–726.

(26) Rusconi, J. M.; Hopkins, S.; Venetta, T. M.; DiMassimo, B.; Cloud, G. A.; Lee, J. Y.; Alldredge, L.; Hunter, E.; Lambert, D.; Bolognesi, D.; Matthews, T.; Johnson, M. R.; Nowak, M. A.; Shaw, G. M.; Saag, M. S. Potent suppression of HIV-1 replication in humans by T-20, a peptide inhibitor of gp41 mediated virus entry. *Nat. Med.* **1998**, 1302–1307.

(27) Chen, L.; Kwon, Y. D.; Zhou, T.; Wu, X.; O'Dell, S.; Cavacini, L.; Hessel, A. J.; Pancera, M.; Tang, M.; Xu, L.; Yang, Z.-Y.; Zhang, M.-Y.; Arthos, J.; Burton, D. R.; Dimitrov, D. S.; Nabel, G. J.; Posner, M. R.; Sodroski, J.; Wyatt, R.; Mascola, J. R.; Kwong, P. D. Structural basis of immune evasion at the site of CD4 attachment on HIV-1 gp120. *Science* **2009**, 326, 1123–1127.

(28) Diskin, R.; Marcovecchio, P. M.; Bjorkman, P. J. Structure of a clade C HIV-1 gp120 bound to CD4 and CD4-induced antibody reveals anti-CD4 polyreactivity. *Nat. Struct. Mol. Biol.* **2010**, 17, 608–613.

(29) Huang, C. C.; Stricher, F.; Martin, L.; Decker, J. M.; Majeed, S.; Barthe, P.; Hendrickson, W. A.; Robinson, J.; Roumestand, C.; Sodroski, J.; Wyatt, R.; Shaw, G. M.; Vita, C.; Kwong, P. D. Scorpion-toxin mimics of CD4 in complex with human immunodeficiency virus gp120 crystal structures, molecular mimicry, and neutralization breadth. *Structure* **2005**, 13, 755–768.

(30) Huang, C. C.; Tang, M.; Zhang, M. Y.; Majeed, S.; Montabana, E.; Stanfield, R. L.; Dimitrov, D. S.; Korber, B.; Sodroski, J.; Wilson, I. A.; Wyatt, R.; Kwong, P. D. Structure of a V3-containing HIV-1 gp120 core. *Science* **2005**, 310, 1025–1028.

(31) Kwong, P. D.; Wyatt, R.; Majeed, S.; Robinson, J.; Sweet, R. W.; Sodroski, J.; Hendrickson, W. A. Structures of HIV-1 gp120 envelope glycoproteins from laboratory-adapted and primary isolates. *Structure (London)* **2000**, 8, 1329–1339.

(32) Kwong, P. D.; Wyatt, R.; Robinson, J.; Sweet, R. W.; Sodroski, J.; Hendrickson, W. A. Structure of an HIV gp120 envelope glycoprotein in complex with the CD4 receptor and a neutralizing human antibody. *Nature* **1998**, 393, 648–659.

(33) Pancera, M.; Majeed, S.; Ban, Y. E.; Chen, L.; Huang, C. C.; Kong, L.; Kwon, Y. D.; Stuckey, J.; Zhou, T.; Robinson, J. E.; Schief, W. R.; Sodroski, J.; Wyatt, R.; Kwong, P. D. Structure of HIV-1 gp120 with gp41-interactive region reveals layered envelope architecture and basis of conformational mobility. *Proc. Natl. Acad. Sci. U.S.A.* **2010**, 107, 1166–1171.

(34) Zhou, T.; Georgiev, I.; Wu, X.; Yang, Z. Y.; Dai, K.; Finzi, A.; Kwon, Y. D.; Scheid, J. F.; Shi, W.; Xu, L.; Yang, Y.; Zhu, J.; Nussenzweig, M. C.; Sodroski, J.; Shapiro, L.; Nabel, G. J.; Mascola, J. R.; Kwong, P. D. Structural basis for broad and potent neutralization of HIV-1 by antibody VRC01. *Science* **2010**, 329, 811–817.

(35) Chen, B.; Vogan, E. M.; Gong, H.; Skehel, J. J.; Wiley, D. C.; Harrison, S. C. Structure of an unliganded simian immunodeficiency virus gp120 core. *Nature* **2005**, 433, 834–841.

(36) Kwon, Y. D.; Finzi, A.; Wu, X.; Dogo-isonagie, C.; Lee, L. K.; Moore, L. R.; Schmidt, S. R.; Stuckey, J.; Yang, Y.; Zhou, T.; Zhu, J.; Vivic, D. A.; Debnath, A. K.; Shapiro, L.; Bewley, C. A.; Mascola, J. R.;

- Sodroski, J.; Kwong, P. D. Unliganded HIV-1 gp120 core structures assume the CD4-bound conformation with regulation by quaternary interactions and variable loops. *Proc. Natl. Acad. Sci. U.S.A.* **2012**, *109*, 5663–5668.
- (37) Starcich, B. R.; Hahn, B. H.; Shaw, G. S.; McNeely, P. D.; Modrow, S.; Wolf, H.; Parks, E. S.; Parks, W. P.; Josephs, S. F.; Gallo, R. C.; Wong-Staal, F. Identification and characterization of conserved and variable regions in the envelope gene of HTLV-III/LAV, the retrovirus of AIDS. *Cell* **1986**, *5*, 637–648.
- (38) Moebius, U.; Clayton, L. K.; Abraham, S.; Harrison, S. C.; Reinherz, E. L. The human immunodeficiency virus gp120 binding site on CD4: delineation by quantitative equilibrium and kinetic binding studies of mutants in conjunction with a high-resolution CD4 atomic structure. *J. Exp. Med.* **1992**, *176*, 507–517.
- (39) Wells, J. A.; McClendon, C. L. Reaching for high-hanging fruit in drug discovery at protein–protein interfaces. *Nature* **2007**, *450*, 1001–1009.
- (40) Fry, D. C. Drug-like inhibitors of protein–protein interactions: a structural examination of effective protein mimicry. *Curr. Protein Pept. Sci.* **2008**, *9*, 240–247.
- (41) Morelli, X.; Bourgeois, R.; Roche, P. Chemical and structural lessons from recent successes in protein–protein interaction inhibition (2P2I). *Curr. Opin. Chem. Biol.* **2011**, *15*, 475–481.
- (42) Vassilev, L.; Fry, D. *Small-Molecule Inhibitors of Protein–Protein Interactions*; Springer: Heidelberg, Germany, 2011; Vol. 348.
- (43) Zhao, Q.; Ma, L.; Jiang, S.; Lu, H.; Liu, S.; He, Y.; Strick, N.; Neamati, N.; Debnath, A. K. Identification of *N*-phenyl-*N'*-(2,2,6,6-tetramethyl-piperidin-4-yl)-oxalamides as a new class of HIV-1 entry inhibitors that prevent gp120 binding to CD4. *Virology* **2005**, *339*, 213–225.
- (44) Madani, N.; Schön, A.; Princiotta, A. M.; Lalonde, J. M.; Courter, J. R.; Soeta, T.; Ng, D.; Wang, L.; Brower, E. T.; Xiang, S. H.; Kwon, Y. D.; Huang, C. C.; Wyatt, R.; Kwong, P. D.; Freire, E.; Smith, A. B., 3rd; Sodroski, J. Small-molecule CD4 mimics interact with a highly conserved pocket on HIV-1 gp120. *Structure* **2008**, *16*, 1689–1701.
- (45) Kolchinsky, P.; Mirzabekov, T.; Farzan, M.; Kiprilov, E.; Cayabyab, M.; Mooney, L. J.; Choe, H.; Sodroski, J. Adaptation of a CCR5-using, primary human immunodeficiency virus type 1 isolate for CD4-independent replication. *J. Virol.* **1999**, *73*, 8120–8126.
- (46) Hoffman, T. L.; LaBranche, C. C.; Zhang, W.; Canziani, G.; Robinson, J. E.; Chaiken, I.; Hoxie, J. A.; Doms, R. W. Stable exposure of the coreceptor-binding site in a CD4-independent HIV-1 envelope protein. *Proc. Natl. Acad. Sci. U.S.A.* **1999**, *96*, 6359–6364.
- (47) Dey, B.; Pancera, M.; Svehla, K.; Shu, Y.; Xiang, S. H.; Vainshtein, J.; Li, Y.; Sodroski, J.; Kwong, P. D.; Mascola, J. R.; Wyatt, R. Characterization of human immunodeficiency virus type 1 monomeric and trimeric gp120 glycoproteins stabilized in the CD4-bound state: antigenicity, biophysics, and immunogenicity. *J. Virol.* **2007**, *81*, 5579–5593.
- (48) Myszka, D. G.; Sweet, R. W.; Hensley, P.; Brigham-Burke, M.; Kwong, P. D.; Hendrickson, W. A.; Wyatt, R.; Sodroski, J.; Doyle, M. L. Energetics of the HIV gp120-CD4 binding reaction. *Proc. Natl. Acad. Sci. U.S.A.* **2000**, *97*, 9026–9031.
- (49) Schön, A.; Madani, N.; Klein, J. C.; Hubicki, A.; Ng, D.; Yang, X.; Smith, A. B., 3rd; Sodroski, J.; Freire, E. Thermodynamics of binding of a low-molecular-weight CD4 mimetic to HIV-1 gp120. *Biochemistry* **2006**, *45*, 10973–10980.
- (50) Yamada, Y.; Ochiai, C.; Yoshimura, K.; Tanaka, T.; Ohashi, N.; Narumi, T.; Nomura, W.; Harada, S.; Matsushita, S.; Tamamura, H. CD4 mimics targeting the mechanism of HIV entry. *Bioorg. Med. Chem. Lett.* **2009**, *20*, 354–358.
- (51) LaLonde, J. M.; Elban, M. A.; Courter, J. R.; Sugawara, A.; Soeta, T.; Madani, N.; Princiotta, A.; Kwon, Y. D.; Kwong, P. D.; Schön, A.; Freire, E.; Sodroski, J.; Smith, A. B., III Design, synthesis and biological evaluation of small molecule inhibitors of CD4-gp120 binding based on virtual screening. *Bioorg. Med. Chem.* **2011**, *19*, 91–101.
- (52) Narumi, T.; Arai, H.; Yoshimura, K.; Harada, S.; Nomura, W.; Matsushita, S.; Tamamura, H. Small molecular CD4 mimics as HIV entry inhibitors. *Bioorg. Med. Chem.* **2011**, *19*, 6735–6742.
- (53) Nonspecificity has been observed (data not shown) for compounds with weak anti-viral activity belonging to the NBD chemotype.
- (54) Schön, A.; Madani, N.; Smith, A. B., III; Lalonde, J. M.; Freire, E. Some drug properties are dependent on thermodynamic signature. *Chem. Biol. Drug Des.* **2011**, *77*, 161–165.
- (55) Haim, H.; Si, Z.; Madani, N.; Wang, L.; Courter, J. R.; Princiotta, A.; Kassa, A.; DeGrace, M.; McGee-Estrada, K.; Mefford, M.; Gabuzda, D.; Smith, A. B., 3rd; Sodroski, J. Soluble CD4 and CD4-mimetic compounds inhibit HIV-1 infection by induction of a short-lived activated state. *PLoS Pathog.* **2009**, *5*, e1000360.
- (56) Wu, X.; Zhou, T.; Zhu, J.; Zhang, B.; Georgiev, I.; Wang, C.; Chen, X.; Longo, N. S.; Louder, M.; McKee, K.; O'Dell, S.; Peretto, S.; Schmidt, S. D.; Shi, W.; Wu, L.; Yang, Y.; Yang, Z. Y.; Yang, Z.; Zhang, Z.; Bonsignori, M.; Crump, J. A.; Kapiga, S. H.; Sam, N. E.; Haynes, B. F.; Simek, M.; Burton, D. R.; Koff, W. C.; Doria-Rose, N. A.; Connors, M.; Mulliken, J. C.; Nabel, G. J.; Roederer, M.; Shapiro, L.; Kwong, P. D.; Mascola, J. R. Focused evolution of HIV-1 neutralizing antibodies revealed by structures and deep sequencing. *Science* **2011**, *333*, 1593–1602.
- (57) Jones, G.; Willett, P.; Glen, R. C.; Leach, A. R.; Taylor, R. Development and validation of a genetic algorithm for flexible docking. *J. Mol. Biol.* **1997**, *267*, 727–748.
- (58) Verdonk, M. L.; Cole, J. C.; Hartshorn, M. J.; Murray, C. W.; Taylor, R. D. Improved Protein–Ligand Docking Using GOLD. *Proteins* **2003**, *52*, 609–623.
- (59) ROCs; OpenEye Scientific Software, Inc. (3600 Cerrillos Road, Suite 1107, Santa Fe, NM 87507), 2008; www.eyesopen.com.
- (60) Grant, J. A.; Gallardo, M. A.; Pickup, B. A fast method of molecular shape comparison. A simple application of a Gaussian description of molecular shape. *J. Comput. Chem.* **1996**, *17*, 1653–1666.
- (61) Rush, T. S., 3rd; Grant, J. A.; Mosyak, L.; Nicholls, A. A shape-based 3-D scaffold hopping method and its application to a bacterial protein–protein interaction. *J. Med. Chem.* **2005**, *48*, 1489–1495.
- (62) Irwin, J. J.; Shoichet, B. K. ZINC—a free database of commercially available compounds for virtual screening. *J. Chem. Inf. Model.* **2005**, *45*, 177–182.
- (63) ZINC, version 7; University of California, San Francisco, CA, 2006; <http://zinc.docking.org/>.
- (64) Monotropic isolates infect cells expressing CD4 and one of the transmembrane co-receptors, CD4/CCR5 or CD4/CXCR4. Dual-tropic isolates can infect cells expressing CD4 and either transmembrane co-receptor CD4/CCR5 or CD4/CXCR4.
- (65) Yuan, W.; Bazick, J.; Sodroski, J. Characterization of the multiple conformational states of free monomeric and trimeric human immunodeficiency virus envelope glycoproteins after fixation by cross-linker. *J. Virol.* **2006**, *80*, 6725–6737.
- (66) Kong, L.; Huang, C. C.; Coates, S. J.; Molnar, K. S.; Skinner, J.; Hamuro, Y.; Kwong, P. D. Local conformational stability of HIV-1 gp120 in unliganded and CD4-bound states as defined by amide hydrogen/deuterium exchange. *J. Virol.* **2010**, *84*, 10311–10321.
- (67) Abad-Zapatero, C.; Metz, J. T. Ligand efficiency indices as guideposts for drug discovery. *Drug Discovery Today* **2005**, *10*, 464–469.
- (68) Bourgeois, R. I.; Basse, M.-J.; Morelli, X.; Roche, X. Atomic Analysis of protein–protein interfaces with known inhibitors: the 2P2I database. *PLoS One* **2010**, *5* (3), e9598.
- (69) Luque, I.; Freire, E. Structure-based prediction of binding affinities and molecular design of peptide ligands. *Methods Enzymol.* **1998**, *295*, 100–127.
- (70) Freire, E. Do enthalpy and entropy distinguish first in class from best in class? *Drug Discovery Today* **2008**, *13*, 869–874.
- (71) Xiang, S. H.; Kwong, P. D.; Gupta, R.; Rizzuto, C. D.; Casper, D. J.; Wyatt, R.; Wang, L.; Hendrickson, W. A.; Doyle, M. L.; Sodroski, J. Mutagenic stabilization and/or disruption of a CD4-bound state

reveals distinct conformations of the human immunodeficiency virus type 1 gp120 envelope glycoprotein. *J. Virol.* **2002**, *76*, 9888–9899.

(72) We did not obtain X-ray cocrystal structure of antipode (–)-6 bound to core gp120.

(73) MOE, *Molecular Operating Environment 2010.10*; Chemical Computing Group: Montreal, Canada, 2010.

(74) Halgren, T. A. MMFF VI. MMFF94s option for energy minimization studies. *J. Comput. Chem.* **1999**, *20*, 720–729.

(75) Halgren, T. A. MMFF MMFF VII. Characterization of MMFF94, MMFF94s, and other widely available force fields for conformational energies and for intermolecular-interaction energies and geometries. *J. Comput. Chem.* **1999**, *20*, 740–774.

(76) Lovell, S. C.; Davis, I. W.; Arendall, W. B., III; de Bakker, P. I. W.; Word, J. M.; Prisant, M. G.; Richardson, J. S.; Richardson, D. C. Structure validation by α geometry: ϕ, ψ and $C\beta$ deviation. *Proteins: Struct., Funct., Genet.* **2003**, *50*, 437–450.

(77) Word, J.; Lovell, S.; Richardson, J.; Richardson, D. Asparagine and glutamine: using hydrogen atom contacts in the choice of side-chain amide orientation. *J. Mol. Biol.* **1999**, *285*, 1735–1747.

(78) Jorgensen, W. L.; Maxwell, D. S.; Tirado-Rives, J. Development and testing of the OPLS all-atom force field on conformational energetics and properties of organic liquids. *J. Am. Chem. Soc.* **1996**, *117*, 11225–11236.

(79) Boström, J.; Greenwood, J. R.; Gottfries, J. Assessing the performance of OMEGA with respect to retrieving bioactive conformations. *J. Mol. Graphics Modell.* **2003**, *21*.

(80) Mills, J. E. J.; Dean, P. M. Three-dimensional hydrogen-bond geometry and probability information from a crystal survey. *J. Comput.-Aided Mol. Des.* **1996**, *10*, 607.

(81) Babcock, G. J.; Mirzabekov, T.; Wojtowicz, W.; Sodroski, J. Ligand binding characteristics of CXCR4 incorporated into paramagnetic proteoliposomes. *J. Biol. Chem.* **2001**, *276*, 38433–38440.

(82) Mirzabekov, T.; Bannert, N.; Farzan, M.; Hofmann, W.; Kolchinsky, P.; Wu, L.; Wyatt, R.; Sodroski, J. Enhanced expression, native purification, and characterization of CCR5, a principal HIV-1 coreceptor. *J. Biol. Chem.* **1999**, *274*, 28745–28750.

(83) Rho, H. M.; Poesz, B.; Ruscetti, F. W.; Gallo, R. C. Characterization of the reverse transcriptase from a new retrovirus (HTLV) produced by a human cutaneous T-cell lymphoma cell line. *Virology* **1981**, *112*, 355–360.

(84) Li, M.; Gao, F.; Mascola, J. R.; Stamatatos, L.; Polonis, V. R.; Koutsoukos, M.; Voss, G.; Goepfert, P.; Gilbert, P.; Greene, K. M.; Bilska, M.; Kothe, D. L.; Salazar-Gonzalez, J. F.; Wei, X.; Decker, J. M.; Hahn, B. H.; Montefiori, D. C. Human immunodeficiency virus type 1 env clones from acute and early subtype B infections for standardized assessments of vaccine-elicited neutralizing antibodies. *J. Virol.* **2005**, *79*, 10108–10125.

(85) Li, M.; Salazar-Gonzalez, J. F.; Derdeyn, C. A.; Morris, L.; Williamson, C.; Robinson, J. E.; Decker, J. M.; Li, Y.; Salazar, M. G.; Polonis, V. R.; Mlisana, K.; Karim, S. A.; Hong, K.; Greene, K. M.; Bilska, M.; Zhou, J.; Allen, S.; Chomba, E.; Mulenga, J.; Vwalika, C.; Gao, F.; Zhang, M.; Korber, B. T.; Hunter, E.; Hahn, B. H.; Montefiori, D. C. Genetic and neutralization properties of subtype C human immunodeficiency virus type 1 molecular env clones from acute and early heterosexually acquired infections in Southern Africa. *J. Virol.* **2006**, *80*, 11776–11790.

(86) Seaman, M. S.; Janes, H.; Hawkins, N.; Grandpre, L. E.; Devoy, C.; Giri, A.; Coffey, R. T.; Harris, L.; Wood, B.; Daniels, M. G.; Bhattacharya, T.; Lapedes, A.; Polonis, V. R.; McCutchan, F. E.; Gilbert, P. B.; Self, S. G.; Korber, B. T.; Montefiori, D. C.; Mascola, J. R. Tiered categorization of a diverse panel of HIV-1 Env pseudoviruses for assessment of neutralizing antibodies. *J. Virol.* **2010**, *84*, 1439–1452.

(87) Wu, X.; Zhou, T.; O'Dell, S.; Wyatt, R. T.; Kwong, P. D.; Mascola, J. R. Mechanism of human immunodeficiency virus type 1 resistance to monoclonal antibody B12 that effectively targets the site of CD4 attachment. *J. Virol.* **2009**, *83*, 10892–10907.

(88) Edgar, R. C. MUSCLE: a multiple sequence alignment method with reduced time and space complexity. *BMC Bioinf.* **2004**, *5*, 113.

(89) Edgar, R. C. MUSCLE: multiple sequence alignment with high accuracy and high throughput. *Nucleic Acids Res.* **2004**, *32*, 1792–1797.

(90) Jones, D. T.; Taylor, W. R.; Thornton, J. M. The rapid generation of mutation data matrices from protein sequences. *Comput. Appl. Biosci.* **1992**, *8*, 275–282.

(91) Kuhner, M. K.; Felsenstein, J. A simulation comparison of phylogeny algorithms under equal and unequal evolutionary rates. *Mol. Biol. Evol.* **1994**, *11*, 459–468.

(92) Huson, D. H.; Richter, D. C.; Rausch, C.; DeZulian, T.; Franz, M.; Rupp, R. Dendroscope: an interactive viewer for large phylogenetic trees. *BMC Bioinf.* **2007**, *8*, 460.

(93) Otwinowski, Z.; Minor, W. Processing of X-ray diffraction data collected in oscillation mode. *Methods Enzymol.* **1997**, *276*, 307–326.

(94) Adams, P. D.; Gopal, K.; Grosse-Kunstleve, R. W.; Hung, L. W.; Ioerger, T. R.; McCoy, A. J.; Moriarty, N. W.; Pai, R. K.; Read, R. J.; Romo, T. D.; Sacchettini, J. C.; Sauter, N. K.; Storoni, L. C.; Terwilliger, T. C. Recent developments in the PHENIX software for automated crystallographic structure determination. *J. Synchrotron Radiat.* **2004**, *11*.

(95) Emsley, P.; Cowtan, K. Coot: model-building tools for molecular graphics. *Acta Crystallogr. D* **2004**, *60*, 2126–2132.

(96) Davis, I. W.; Leaver-Fay, A.; Chen, V. B.; Block, J. N.; Kapral, G. J.; Wang, X.; Murray, L. W.; Arendall, W. B., 3rd; Snoeyink, J.; Richardson, J. S.; Richardson, D. C. MolProbity: all-atom contacts and structure validation for proteins and nucleic acids. *Nucleic Acids Res.* **2007**, *35*, W375–W383.

(97) Delano, W. PyMOL 098; DeLano Scientific LLC: South San Francisco, CA; <http://www.pymol.org>. This is an open-source molecular graphics system developed, supported, and maintained by DeLano Scientific LLC (<http://www.delanoscientific.com>).